

1-1-2013

Modeling Of Mouse Eye And Errors In Ocular Parameters Affecting Refractive State

Gurinder Bawa
Wayne State University,

Follow this and additional works at: http://digitalcommons.wayne.edu/oa_dissertations

 Part of the [Electrical and Computer Engineering Commons](#), and the [Optics Commons](#)

Recommended Citation

Bawa, Gurinder, "Modeling Of Mouse Eye And Errors In Ocular Parameters Affecting Refractive State" (2013). *Wayne State University Dissertations*. Paper 749.

This Open Access Dissertation is brought to you for free and open access by DigitalCommons@WayneState. It has been accepted for inclusion in Wayne State University Dissertations by an authorized administrator of DigitalCommons@WayneState.

**MODELING OF MOUSE EYE AND ERRORS IN OCULAR PARAMETERS
AFFECTING REFRACTIVE STATE**

by

GURINDER BAWA

DISSERTATION

Submitted to the Graduate School

of Wayne State University

Detroit, Michigan

in partial fulfillment of the requirements

for the degree of

DOCTOR OF PHILOSOPHY

2013

MAJOR: ELECTRICAL ENGINEERING

Approved by:

Advisor

Date

© COPYRIGHT BY

GURINDER BAWA

2013

All Rights Reserved

DEDICATION

Dedicated to

My father Jagjit Singh Bawa, mother Swinderjit Kaur and dearest wife Simerjeet Kaur for their
endless support and Love

&

To my late grandfather Gurbaksh Singh Bhalla and late grandmother Agya Wanti.

ACKNOWLEDGEMENTS

First and foremost, above all I would like to express my sincere gratitude to my principal advisor Dr. Ivan Avrutsky, who always stood by me during the time of need, while advising me. I am really thankful to him for extending his valuable, time, guidance and advice. I am grateful to all my committee members Dr. Andrei Tkatchenko, Dr. Mark Cheng and Dr. Amar Basu for their valuable advice and agreeing to be on my dissertation committee. I extend my thanks to Graduate program director Dr. Syed Mahmud and Dr. Han for their valuable advice. I also want to thank School of Medicine, Wayne State University, at Detroit for providing the valuable information that flourished to valuable and productive results.

I would like to express my gratitude towards George Tecos for his continuous support and motivated me for research. I also want to thank fellow graduate students in the Optoelectronics Research Group, Sabarish Chandramohan, Steve, Mohammad Hossain, and former graduate student Pradeep Kumar for their help and co-operation. I also thank Cynthia Lee Sokol, Betsy Baumann and PhD Office staff for their friendly nature and extreme patience. I would also like to thank the ECE Staff and department secretary, Dories R. Ferrise and Graduate Advisor Sofia O. Malynowskyj from OISS office for their help.

My special thanks to all my friends and fellow graduate students Hardeep Singh, Kulbir Singh, Kshitij Sharma, Anil Kumar and Ajay Kumar for their ever good company, cheering and support during the final days. I owe my special gratitude to former class mate and my best friend who helped me to learn life and encouraged me to take challenges in life.

At last but not the least I thank all my friends, Dr. Mohan Singh, Manjit Singh, Narpinder Chahil, Vishal Narang, Pardeep Kumar, Sanjeev, Devinder Singh and Ankit Saxena and my

family especially my brothers and Sister (Parminder, Raminder and Gagandeep) for their love, encouragement and good spirits.

PREFACE

In this dissertation, I have presented my work on Modeling of an eye and aberrations in ocular parameters affecting refractive state. In the first part of the dissertation, Modeling of an eye using sophisticated algorithms is performed and model is authenticated by verifying the model. Second part of dissertation discussed the Ray tracing models using concepts of geometry. In the final part of my dissertation I have performed Variational Analysis to validate the model qualitatively as well as quantitatively.

Chapter 1 begins with the introduction of an Eye, its optical properties and formation of image from optics point of view. Subsequently we have overviewed the different methodologies adopted by researchers to obtain ocular parameters and observed errors in the refractive state of an eye. In the later parts we have introduced the concept of modeling of an eye, extraction of ocular components followed by verification of the model. Concept of ray tracing using these ocular parameters was introduced. In the last part of chapter 1 the idea of variational analysis would explain the procedure of how the targeted work was achieved.

Chapter 2 describes the process of Modeling of an eye. In this chapter the raw data provided by School of Medicine was used to build the model of an eye using state of the art algorithms. Ocular parameters and schematics of an eye consisted of different layers were generated. The statistical data was generated as well, which helped in validation of the model.

Chapter 3 deals with the Image processing part, in which MRI images of an Eye was overlapped with the respective schematics of an eye, resulting in a composite image of an eye. This was performed further to validate the model of an eye.

In chapter 4 the introduction of concept of Ray tracing using Ocular parameters, became inevitable because of the nature of research performed. In this part the ocular parameters just

generated while performing Modeling of an Eye, were inserted in the mathematical equations for ray tracing. This would give us a virtual eye in 2 dimensions in paraxial approximation, in which it is shown that paraxial rays after entering the eye and traveling a certain distance meet at a focal point. Depending upon the focal point, disorder (myopia or hyperopia) and how much magnitude could be calculated.

Chapter 5 eventually proceeds to complement our work by qualitatively as well as quantitatively analyzing the result. In this chapter we would analyze those ocular parameters which have stronger or weaker impact on the refractive state of an eye and are categorized accordingly in critical or non-critical category.

Chapter 6, 7 and 8 discuss the results of the work performed by us, discussion of the results and conclusion respectively.

Sincerely,

Gurinder Bawa.

TABLE OF CONTENTS

Dedication	ii
Acknowledgments	iii
Preface	v
List of Tables	x
List of Figures	xi
Chapter 1. Introduction	1
1.1 Motivation	3
1.2 Schematics of an Eye	4
1.3 Image Processing	7
1.4 Ray Tracing	8
1.5 Variational Analysis	10
Chapter 2. Schematics and Geometry of Eye	15
2.1 History of Eye Modeling	15
2.2 Schematic of an Eye	17
2.3 Modeling of an Eye	19
2.3.1 Plot X-Y Coordinates	19
2.3.2 Smooth Curve Fitting	22
2.3.3 Goodness of Curve	23
2.3.4 Centers of Curvature, Radii and other Ocular Parameters	23
2.3.5 Average of Ocular Parameters	28
2.3.6 Average Schematic of an Eye	30
Chapter 3. Image Processing	31

3.1 Locate the Images	32
3.2 Rotation of MRI image and overlapping of two images	33
3.3 Visual Analysis	37
Chapter 4. Optical Modeling and Ray Tracing	38
4.1 Computational Model of ray tracing	41
4.1.1 Ocular Parameters of Mouse and Rat eye	41
4.1.2 Ray Tracing	46
Chapter 5. Refractive Error and Variational Analysis	53
5.1 Refractive Error	53
5.2 Variational Analysis	56
Chapter 6. Results	59
6.1 Results of Schematics and Geometry of an Eye	60
6.1.1 Ocular Data	60
6.1.2 Schematics of an Eye	63
6.2 Results of Image Processing	65
6.3 Results of Optical Modeling and Ray Tracing	67
6.4 Results of Variational Analysis	69
Chapter 7. Discussion	75
7.1 Schematics of an Eye	75
7.2 Image Processing	76
7.3 Optical Modeling and Ray Tracing	76
7.4 Variational Analysis	77
Chapter 8. Conclusion	81

References	82
Abstract	87
Autobiographical Statement	89

LIST OF TABLES

Table 1.1	Summary of Different Strains of Mice used in Experiment	5
Table 1.2	Tabulated above are ocular parameters that are used for calculation of Refractive error	11
Table 1.3	Summary of representation of derivatives of ocular parameters	13
Table 2.1	X-Y coordinates of Posterior Corneal Layer of M2_L mice of C57BL . . .	20
Table 2.2	Summary of notations used in the model	28
Table 4.1	Summary of Ocular parameters of rat Eye. Values of Refractive indices are taken at wavelengths ranging from 475nm to 650nm with regular interval of 25nm	42
Table 4.2	Summary of Ocular parameters of mouse Eye. Values of Refractive indices are taken at wavelengths 488nm, 544nm, 596nm, 655nm with regular interval of 25nm	43
Table 4.3	Summary of ocular parameters of C57BL mouse strain averaged over all specimens	44
Table 4.4	Summary of ocular parameters of C57L mouse strain averaged over all specimens	44
Table 4.5	Summary of ocular parameters of CE mouse strain averaged over all specimens	45
Table 4.6	Summary of ocular parameters of CZECH mouse strain averaged over all specimens	45
Table 5.1	Notations for ocular parameters and their respective derivatives	58
Table 6.1	Variational Analysis for Rat eye [3, 4, 5] at wavelengths ranging from 475-650nm at a regular interval of 25 nm	70
Table 6.2	Variational Analysis for Mouse eye [6, 7] at wavelengths 488nm, 544nm, 596nm and 655nm	71
Table 6.3	Variational Analysis for C57BL mouse eye strain at wavelengths 500nm and 510nm	72

LIST OF FIGURES

Figure 1.1	Schematic of an eye with all 6 refractive surfaces. From left to right the name of the surfaces are anterior cornea, posterior cornea, anterior lens, posterior lens, anterior retina and posterior retina respectively	6
Figure 1.2	Overlapping of two Images. Red part shows the layers generated by our model and behind that is MRI image of a mouse eye	8
Figure 1.3	Paraxial rays that are entering in an eye are finally focusing at focal point. The origin of paraxial rays is at $-\infty$	10
Figure 2.1	Schematic of an eye consisting of different surfaces and other parts.	17
Figure 2.2	Schematic of an eye of #M1_L specimen of mice strain C57BL	21
Figure 2.3	Image of an eye of #M1_L specimen of mice strain C57BL after transformation	22
Figure 2.4	Arc from where co-ordinate points (X_c, Y_c) for center of radii of curvature are calculated using geometry	24
Figure 2.5	Schematic and Summary of an eye with ocular parameters. Surfaces are notated by letter S. $S_0, S_1, S_2, S_3, S_4, S_5$, are Surfaces of anterior cornea, posterior cornea, anterior lens, posterior lens, anterior retina and posterior retina respectively. Thickness or depths are represented by tt and $tt_1, tt_2, tt_3, tt_4, tt_5$ are thicknesses of cornea, aqueous chamber, lens, vitreous chamber and retina respectively. C represents center of curvature and is clear from subscript $C_c, C_{al}, C_{pl}, C_{ar}, C_{pr}$ and center of curvatures for cornea, anterior lens, posterior lens, anterior retina and posterior retina.	27
Figure 2.6	Schematic of an eye of C57BL mice strain drawn as a result of all the ocular parameters averaged over all 6 specimens of the same strain	30
Figure 3.1	The MRI image of an eye. Along with the eye ball other surrounding tissues and blood vessels are also visible	33
Figure 3.2	Image after rotating 90 degrees to the left	34
Figure 3.3	Different plotted layers of an eye	35
Figure 3.4	Overlapping of MRI image and layers drawn from the raw points. MRI image served as background and layers drawn in red are on top of that	36

Figure 3.5	Composite image of Region of interest in an eye	37
Figure 4.1	Schematic of an eye with different layers and their respective refractive indices	40
Figure 4.2	Paraxial schematic model of emmetropic rodent eye	48
Figure 5.1	Virtual Eye comprising of different layers with condition of myopia	54
Figure 5.2	Virtual Eye comprising of different layers with condition of hyperopia	55
Figure 6.1	Summary of the ocular components of specimen M1_L of strain C57BL	61
Figure 6.2	Summary of the ocular components of specimen M1_L of strain C57BL	62
Figure 6.3	Summary of the ocular data averaged over all specimens of strain C57BL	63
Figure 6.4	Schematic of an eye for specimen M1_L	64
Figure 6.5	Schematic of an eye for C57BL averaged over all the 6 specimens	64
Figure 6.6	MRI image of an eye	65
Figure 6.7	6 different layers of an eye representing schematic of an eye	66
Figure 6.8	Composite image showing the overlapped part in red on top of MRI image	66
Figure 6.9	Summary of eye parameters calculated in paraxial approximation for rat eye [3, 4, 5]	67
Figure 6.10	Summary of eye parameters calculated in paraxial approximation for mouse eye [6, 7]	68
Figure 6.11:	Summary of eye parameters calculated in paraxial approximation for C57 mouse strain	69

CHAPTER 1

INTRODUCTION

Eyes, the smallest part, yet the imperative organ of a body give a sense of vision to living creatures. The light rays that enter through pupil of an eye, travelling through different layers, consisting of different refractive indices, converges at a far end point of an eye. This point of convergence of light rays is called as focal point of an eye and usually lies at the posterior part of retina or more precisely sensory part of retina. This sensory part relays signal to optic nerves located next to retina which in turn acts as messenger and sends the signal to brain [1]. Finally we see image after the processing of signal is completed by brain.

While we talk about image formation, it is necessary that the focal point should be in the neighborhood of photoreceptive layer of retina, where later senses the light signal and sends the information to optics nerve. Sometimes the image formation is perfect and is distinguishable for its character, but sometimes the image is blurred due to number of reasons. Hence there is a certain disorder related with the power of an eye, named as “Refractive Error” or “Ametropia” of an eye [2]. Those refractive errors lead many researchers [3-5, 7, 8-12, 16-26] to put significant efforts to understand the factors that contribute towards the refractive error. Different animal models, such as Rodents [3-24], Chicken [25, 26], Avian [27] and Rabbit [28] have been used to understand the behavior.

Amongst all the above mentioned animal models, Rodents (Mouse and Rat) model has been under extensive study because of the fact that it is easy to be affordable in terms of fast reproduction, cost-effective, variable models and its acceptance towards genetic mutation. Besides above explained reason these models are studied also for, normal development of eye and other pathological conditions that affects visual system, because of the analogy of

physiological and genetically similar organization to those of humans. The experiments on mice eyes have shown that they are the most suitable models for the calculation of refractive eye development.

Many researchers not only have contributed towards the anatomy and physiology of an eye but various optical models have been proposed to understand the schematics. They had also reported ocular parameters such as radii of curvature, thicknesses and refractive indices of mouse eyes. Despite of the efforts put forth these models are considered to be less reliable due to variability in reported ocular parameters. Due to variability in the reported ocular parameters the refractive error of a mouse eye suffers.

Several experiments have been conducted on mouse and rat eyes using preserved sections and refractive indices that are obtained from ray tracing experiments. These experiments are eventually used to study the biometry and schematics of eyes. Hughes [3], Campbell and Hughes [4] and Chaudhari et al [5] put forth the schematics of rat eye model and calculated the ocular parameters as well. Similarly Remtulla and Hallet [6] and Schmucker and Schaeffel [7] conducted experiments on mouse eye and proposed model for schematic of eye. Those studies have reported averages of radii of curvatures, thicknesses of different layers of an eye and refractive indices at different wavelengths. Further they have also calculated refractive errors using ray tracing models at different wavelengths. In addition to that Remtulla and Hallet [6] have compared other parameters of mouse eye to rat eye, such as linear scale, magnification factor and refractive indices. X. Zhou et al. [8] and E. G. de la Cera et al. [9] predicted that imaging at high resolution of rodent eyes, is complicated by high optical power and high spherical aberrations of an eye, using adaptive optics. However Geng et al [10] found that optical

quality is better in mouse eye as compared to that of human eyes because of larger numerical aperture and similar magnitude of RMS higher order aberrations.

Although above mentioned studies have been acknowledged for providing basic information about optical properties of rodent eyes as well as schematics of an eye, yet there is great uncertainty while validating the refractive error of the eye due to variability in the reported ocular parameters. Variability prevails even in the reported data for the same strains of mice as is shown by G. Zhou, and R. W. Williams [11], A. V. Tkatchenko et al. [12] and M. T. Pardue et al. [13]. Such a similar case is reported in [12], where significant differences are reported between C57BL/6J, C57L/J and CZECHII/EiJ mice strains for corneal radius of curvature, Vitreous chamber depth and refractive error. There is also variability in refractive errors reported in most commonly C57BL/6 mice. Even though different experiments predicted that, refractive error reported in C57BL/6 mice are close to zero [14-21], still other studies reported either hyperopia (4.1-6.4 D) or myopia (5.6-9.2 D) in same strain of mice [7, 10, 22-24].

1.1 Motivation

Despite of the fact that there is variability in reported optical properties of an eye, yet these models holds valid and are contributing significantly in their respective areas. But none to our knowledge had ever tried to analyze the factors that are affecting the calculations of refractive errors and which particular ocular parameter is responsible for incorporating difference in refractive error. Such a model which could qualitatively predict the abnormal behavior of an eye would not only help us in understanding the optics of an eye but would also help us predict the aberrations due to single parameter. This challenge motivated us to conduct the experiments on mouse eyes from above described animal models. The reason that we have chosen mouse

eyes from rodents family instead of rat or other species because of the fact that mice models are genetically engineered models with enough variance. Also the genetic organization is similar to that of humans. Hence this project is a part of research ultimately aimed at understanding genetic predisposition for myopia in humans.

In our work we had emphasized the importance of small aberrations in optical parameters, which could lead to significant changes in refractive error of mouse eye. We have built a model for a mouse eye that is smart enough to calculate the optical parameters of an eye such as thicknesses and radii of curvatures of different surfaces of an eye. The calculated optical parameters are then used to draw the schematics of an eye. Also the refractive error of an eye is calculated using those optical parameters. Finally to meet the challenge Variational analysis is performed in order to study the effects on the refractive error of an eye if an optical parameter is changed by the smallest possible value. This variational analysis helped us to identify those ocular parameters which have higher impact as well as those parameters which are having smaller influence on refractive state and refractive error of rodent eyes.

1.2 Schematics of an eye

Above stated work was performed with the help of School of Medicine, Wayne State University. Dr. Andrei Tkatchenko, from department of Ophthalmology provided us the necessary data required for the modeling. X and Y coordinates from MRI images of a mouse eye, using Image J software, were extracted which served as the basic building block of our work. X-Y coordinates define different layers that are present in the mouse eye. Ocular dimensions of four strains of mouse eye were given to us, viz. a viz. C57BL, C57L, CE and CZECH. Strain is defined as the genetically mutated species. Further each strain has number of specimens that

contain ocular data. Table 1.1 summarizes the different strains and names of their corresponding specimens used in our work.

Strains of Mice Eye	Number of Specimens	Names of the Specimens
C57 BL	6	1. M1_L 2. M2_L 3. M3_L 4. L1_L 5. L4_L 6. # M1_L
C57 L	5	1. 10-1 2. 23-1 3. 28-1 4. 33-1 5. 38-1
CE	4	1. 14-1 2. 27-1 3. 36-1 4. 43-1
CZECH	4	1. 11-1 2. 15-1 3. 22-1 4. 28-1

Table 1.1: Summary of Different Strains of Mice used in Experiment.

In order to make schematics as well as to obtain the ocular parameters of each specimen of strain of the mouse eye we have to build a model that is capable of inputting the ocular dimensions and performs the former task. This tedious job was performed by writing number of programs using MATLAB. Those programs written in MATLAB are smart enough that they are able to locate the file where all the ocular dimensions of the different specimens of all the strains are present. After locating files, the data for each surface of an eye is fetched and schematic of an

eye with 6 refractive surfaces is plotted with the help of sophisticated code. Figure 1.1 below shows the schematic of an eye drawn from the ocular coordinates of an eye. Not only the image

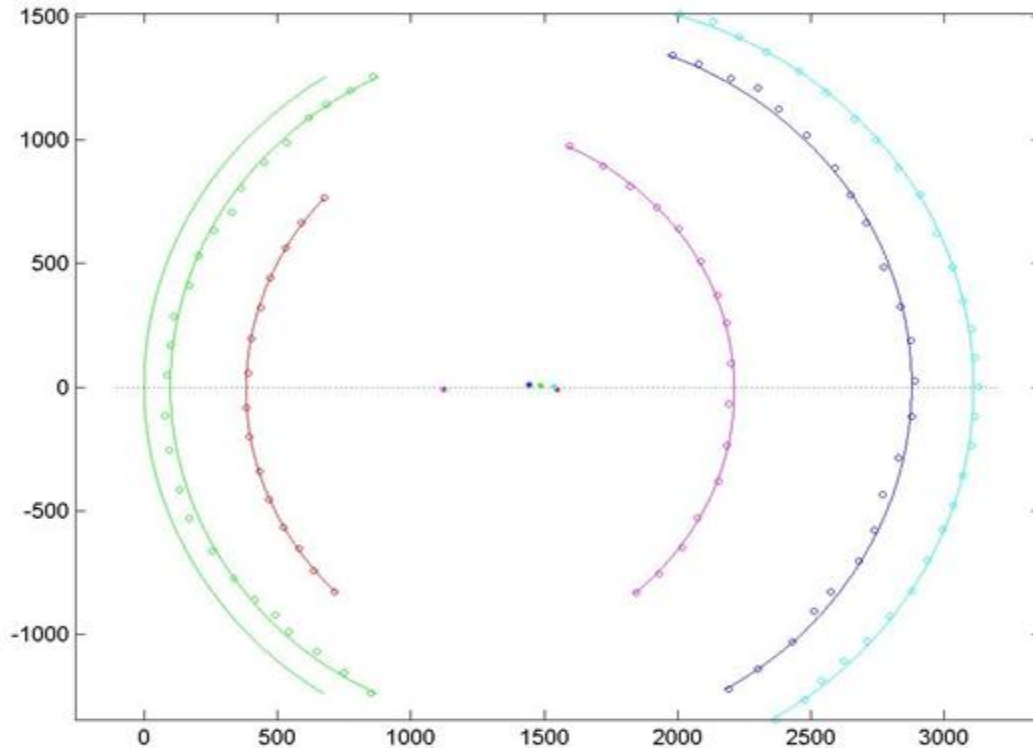


Figure 1.1: Schematic of an eye with all 6 refractive surfaces. From left to right the name of the surfaces are anterior cornea, posterior cornea, anterior lens, posterior lens, anterior retina and posterior retina respectively.

containing 6 layers is drawn but also other important ocular parameters, such as radii of curvature, center points of curvature, thicknesses of different surfaces etc., required for the ray tracing were obtained. Circular points overlaying on each surface represents the actual raw points or we can say the X-Y coordinates of an eye. Dashed line passing through all surfaces is an optical axis and dotted colored points on optical axis represent centers of curvature of corresponding layers. With the help of algorithms we have performed the following steps in sequence:

1. Plot the X-Y coordinates.
2. Smooth curve fitting.
3. Calculated goodness of the curve fitting.
4. Calculated ocular parameters (Radii of Curvature, Thicknesses of surfaces, Center Points)
5. Average* of radii of curvature and thicknesses of surfaces.
6. Schematic of an eye averaged over all specimens of single strains.

*Note: *As already mentioned that we have 4 strains of mice and each strain has number of specimens. In step 5 we have averaged all the specimens of corresponding single strain.*

1.3 Image processing

Now we have drawn the schematics of an eye using the X-Y coordinates of ocular parameters, next thing to do is validate the model that is built with the help of code using sophisticated algorithm. As already mentioned, that these ocular coordinates were extracted from the MRI images of a mouse eye, so we can compare the original MRI images with the images that were drawn by our model. For that purpose we wrote program that could overlap the image of the schematic that we built and the MRI image of the corresponding specimen of the mouse eye.

The concept of overlapping of the two images helped us to visually analyze and detect if the model built for the schematic of an eye from ocular coordinates suffices or not. Figure 1.2 shows the overlapped image of MRI image of an eye with different layers and the schematic of an eye of that is generated from the simulation of our model. We can see that both the images are overlapping perfectly with minor offset at the edges which could be accounted for the error while extracted ocular coordinates.

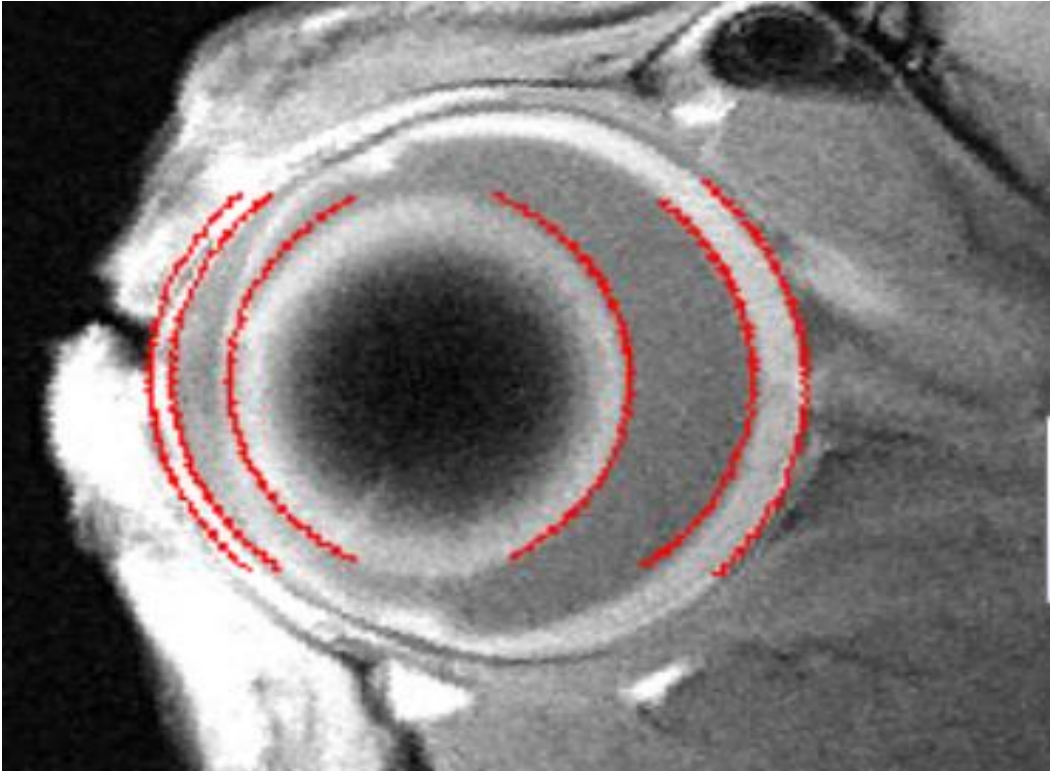


Figure 1.2: Overlapping of two Images. Red part shows the layers generated by our model and behind that is MRI image of a mouse eye.

1.4 Ray Tracing

Ray tracing is a method used to determine paths traveled by waves or particles. These waves travel with certain velocity while passing through different media. These media could more precisely be characterized by refractive indices. The media are separated by different refractive surfaces. One is able to see an object, when beams of light hit an object and after adhering to basic laws of reflection as well refractions, the rays enter in our eyes through pupil. The light rays that are going to enter in our eyes are about to follow the laws of optics and hence we would be able to see the object. As the behavior of perception of eyes of all living creatures is similar, so is the case of mice eyes. There are three different models of a mice eye that are

proposed by Remtulla and Hallet [6]. Those three models of mouse eye are “Homogeneous” Model, “Heterogeneous” Model and “Core” Model. All three models are responsive to small errors in r , tt , and n . The ametropia of an eye and geometrical parameters as well are calculated. Out of those above mentioned models we have considered homogeneous model as it is less complicated and requires fewer measurements.

A homogeneous model of an eye has 6 refractive surfaces. The name of the layers from front to back of an eye are arranged in the order of anterior cornea, posterior cornea, anterior lens, posterior lens, anterior retina and posterior cornea. The main volume of an eye is occupied by lens, followed by vitreous chamber, aqueous chamber and retina respectively. As image formation principle applies to any combination of convex lenses or any living creature so is the case with rodents. Snell’s law comes into play as we talk of image formation through different planes with different refractive indices. After obeying all the physical laws of optics the rays finally meet at the back surface of retina or more precisely sensory part of retina. The optic nerves carry the information to central processing unit of brain and after processing the information rodents can finally see the image formation

A cone of rays emanating from source, which is at infinite distance from the lenses and the rays that travel parallel to optical axis are called as paraxial rays. Paraxial rays after travelling through different surfaces of any eye meets at a focal point of an eye. For a perfect eye ($A=0$ diopters) all the rays converge at sensory point of posterior retina and that eye is free of any refractive error. In myopic eye ($A<0$ diopters) the rays converge in front of retina, whereas in case of hyperopic eye ($A>0$ diopters) rays meet behind the retina. Figure 1.3 shows the schematic of a perfect eye where paraxial rays are entering an eye and after refractions through different surfaces the rays are focusing at focal point of an eye.

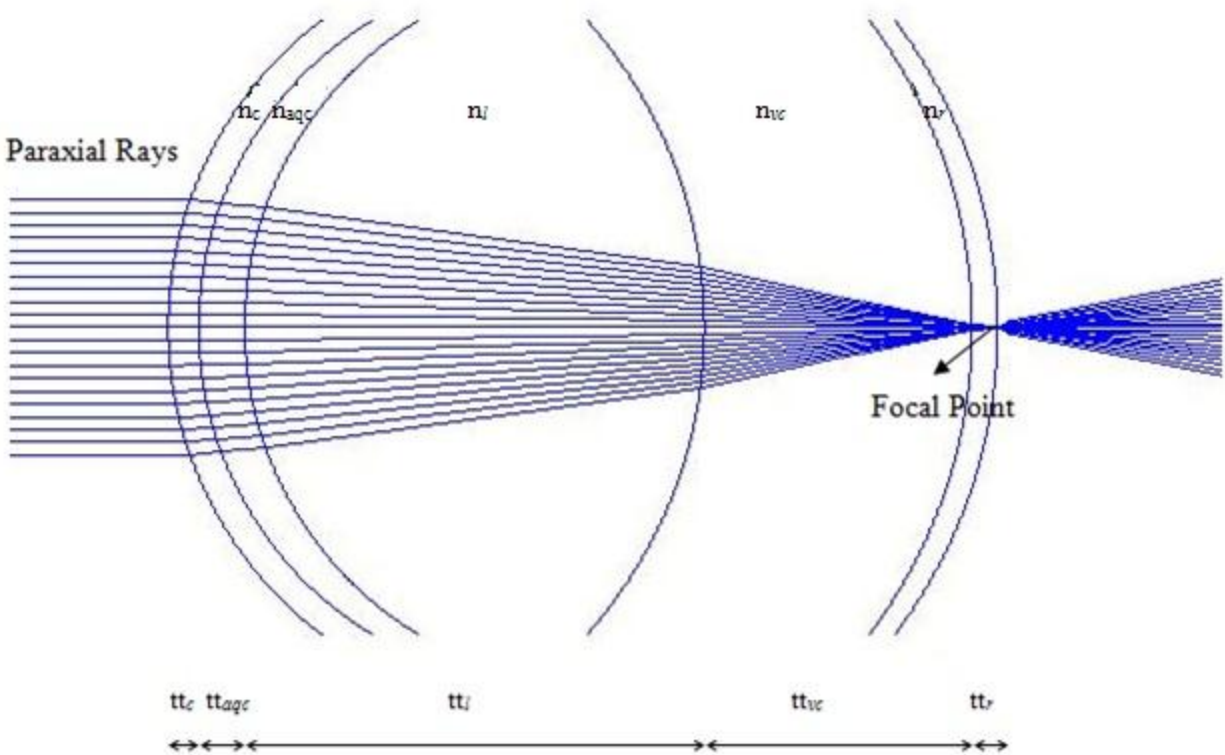


Figure 1.3: Paraxial rays that are entering in an eye are finally focusing at focal point. The origin of paraxial rays is at $-\infty$.

The ray tracing model in our studies is based on exact solutions for the rays in accordance with Snell's law of refraction and it is not limited to paraxial rays only. With properly quantified output the same ray tracing core is suitable for studying wide-angle aberrations, image distortion, and other imaging imperfections. A particular task at the moment was to study eye ametropia in paraxial approximation, so only close-to-axis rays were considered.

1.5 Variational Analysis

We know that how the rays ideally would converge at the focal point of an eye and hence a sharp image is formed. But ideal condition is just an imagination and we have to go beyond

this imagination as ideal conditions do not prevail all the time. As we had calculated ocular parameters from the schematics of an eye and also we know how the ray tracing is performed, the next task to be performed is to analyze that how the rays would be focused if we would incorporate all those calculated parameters. The rays can focus at the retina which we say is an ideal condition, but sometimes it could be in front of retina (photoreceptor area) or behind the retina.

The rays that converge in front of retina or had a focal point in front of retina is associated with the defect known as myopia (short sightedness). Hyper-myopia is a condition when the focal point is behind the retina. We can notice that there is some error associated with an eye which is usually called as a refractive error of an eye. In other words we can also call it as “Ametropia”. Using all the 16 ocular parameters which are summarized in table 1.2 we can calculate Ametropia (A) or refractive error of an eye.

Ametropia as a function of		
Radii of Curvature of	Thickness or Depth of	Refractive Index of
1. Anterior Cornea (r_{ac})	1. Cornea (tt_c)	1. Cornea (n_c)
2. Posterior Cornea (r_{pc})	2. Aqueous Chamber (tt_{aqc})	2. Aqueous Chamber (n_{aqc})
3. Anterior Lens (r_{al})	3. Lens (tt_l)	3. Lens (n_l)
4. Posterior Lens (r_{pl})	4. Vitreous Chamber (tt_{vc})	4. Vitreous Chamber (n_{vc})
5. Anterior Retina (r_{ar})	5. Retina (tt_r)	5. Retina (n_r)
6. Posterior Retina (r_{pr})		

Table 1.2: Tabulated above are ocular parameters that are used for calculation of Refractive error.

Hence we can say that ametropia is a function of 16 parameters and can be represented by notation as shown below in Eq. 1.1.

$$A = f(r_{ac}, r_{pc}, r_{al}, r_{pl}, r_{ar}, r_{pr}, tt_c, tt_{aqc}, tt_l, tt_{vc}, tt_r, n_c, n_{aqc}, n_l, n_{vc}, n_r) \quad (1.1)$$

In literature, as already discussed everyone had experimented on different animal models and discussed about the refractive error and mostly the work is done on mice models [3-22]. The values of refractive error calculated are not same even in the same strains of mice. Some of the researchers say that C57BL/6 mice have refractive errors close to zero diopters [12-19] while others say that mice of same strain are myopic or hyperopic [5, 8, 20-22]. Even though there is so much variability in the refractive errors no one has ever tried to qualitatively analyze the factors that are affecting the refractive state of an eye. This qualitative analysis will not only allow us to detect the parameters which are responsible for variable refractive error but it would also help us in better understanding the optics of an eye as well as refractive state.

This concept leads us to do “Variational analysis”. As the name indicates ocular parameters are varied and the results for ametropia are obtained as a result of this variation. In variational analysis one out of the 16 above tabulated ocular parameters is incremented by a small variable value, while keeping all other fixed. Let us assume that the ametropia calculated by above step is called as A1 and the original ametropia is A. Thus the difference between original ametropia A and A1 gives us the change in value of ametropia due to increment of single ocular parameter. This change in value of ametropia is called as the derivative of that ocular parameter. For better understanding we can assume that we are incrementing the radius of curvature of anterior cornea by a small value. Thus the derivative for radius of curvature anterior cornea can be represented by Eq. 1.2.

$$dA_{dr_{ac}} = A1 - A$$

1.2

Ocular Parameters of		DERIVATIVES
Radius of curvature of	1. Anterior Cornea	$dA_{dr_{ac}}$
	2. Posterior Cornea	$dA_{dr_{pc}}$
	3. Anterior Lens	$dA_{dr_{al}}$
	4. Posterior Lens	$dA_{dr_{pl}}$
	5. Anterior Retina	$dA_{dr_{ar}}$
	6. Posterior Retina	$dA_{dr_{pr}}$
Thicknesses or depths of	1. Cornea	dA_{dtt_c}
	2. Aqueous Chamber	$dA_{dt_{aqc}}$
	3. Lens	dA_{dtt_l}
	4. Vitreous Chamber	$dA_{dtt_{vc}}$
	5. Retina	dA_{dtt_r}
Refractive Index of	1. Cornea	dA_{dn_c}
	2. Aqueous Chamber	$dA_{dn_{aqc}}$
	3. Lens	dA_{dn_l}
	4. Vitreous Chamber	$dA_{dn_{vc}}$
	5. Retina	dA_{dn_r}

Table 1.3: Summary of representation of derivatives of ocular parameters.

This variational analysis allowed us to thoroughly investigate the parameters that have great impact on ametropia and can be categorized as crucial or critical parameters. Also we can detect those ocular parameters which have little or practically no impact on ametropia and are less critical. Table 1.3 is constructed to represent all the possible derivatives of an eye for the respective ocular parameter.

CHAPTER 2

SCHEMATICS AND GEOMETRY OF EYE

A schematic of an eye represents the geometrical aspect where all the information regarding radius of curvature, center of radius of curvature, thicknesses of different surfaces and other optical properties can be acknowledged. It refers to the mathematical model that is built on the basis of optical features of an eye. A simple basic model is deprived of all the complex situations such as aspheric surfaces and is built on few assumptions. Schematic of an eye models are mere approximations to real eyes as they only use spherical surfaces and constant refractive indices of lens. However a real eye has aspheric surfaces and gradient refractive index of a lens. “Finite aperture” or “wide angle” schematic eyes are those in which schematic of eyes are made accurate by introducing one or more aspheric surfaces along with a lens having gradient refractive index. Based on all those assumption many models of schematic of eye are present in literature and some of the models are discussed in the preceding section.

2.1 History of Eye Modeling

Ever since the first model of an eye which was given by Christian Huygens, many models of an eye have been proposed till date. The simplified Gullstrand model, theoretical eye of LeGrand and simplified theoretical eye of LeGrand [29] are considered to be simple models representing an eye. All three models are alike in terms of radii of curvatures, thicknesses of surfaces and refractive indices of medium except few changes. In first two models cornea and anterior chamber have a distinguishable boundary and lens is represented by simple pair of surfaces having finite thickness, whereas in later case the cornea and anterior chamber are fused having finite thickness and is considered to have an ideal disappearing thickness.

In full Gullstrand eye model [30] the lens is consisted of a kernel and a shell capsule and it is characterized by four refracting surfaces. The refractive power is changed by variations in radii and distances. The eye model of Walker [31] is similar to simple Gullstrand model with minor changes in the values of ocular parameters. Generalized reduced eye [30] is a continuation of the early work of reduced eye model of Emsley [32], where in later case it was assumed that only one refracting surface is required to explain the behavior of an eye. In generalized reduced eye front surface is made aspherical in addition to introduction of pupil to realize the field effects description.

Models given by Kooijman [33] and Navarro [34] consist of four aspherical surfaces and with the help of this model they were able to explain accommodation, chromatic behavior and spherical aberrations. In extended work of I. Escudero-Sanz [35], the wide angle properties of an eye were also considered. The eye model given by Liou-Brennan [36] also uses aspherical surfaces along with dual gradient media and described spherical aberration and disorder of eye, astigmatism flawlessly. Although all the above mentioned models have difference in their overlay but still there is uniqueness in terms of the dimensions of ocular parameters that are cited by everyone.

Most of the models which are discussed above have mentioned four refractive surfaces, i.e., two for cornea as well as two for lens. We have worked on a model that is similar to Gullstrand eye, where we had elaborated the model by distinguishing the anterior and posterior parts of every surface. Each surface of an eye has finite thickness and is separable by definite boundary. Also there is retinal part that is included in order to accurately observe the behavior of an eye and hence the defects associated with that. Figure 2.1 shows the structure of an eye with all the 6 layers that are used in our case.

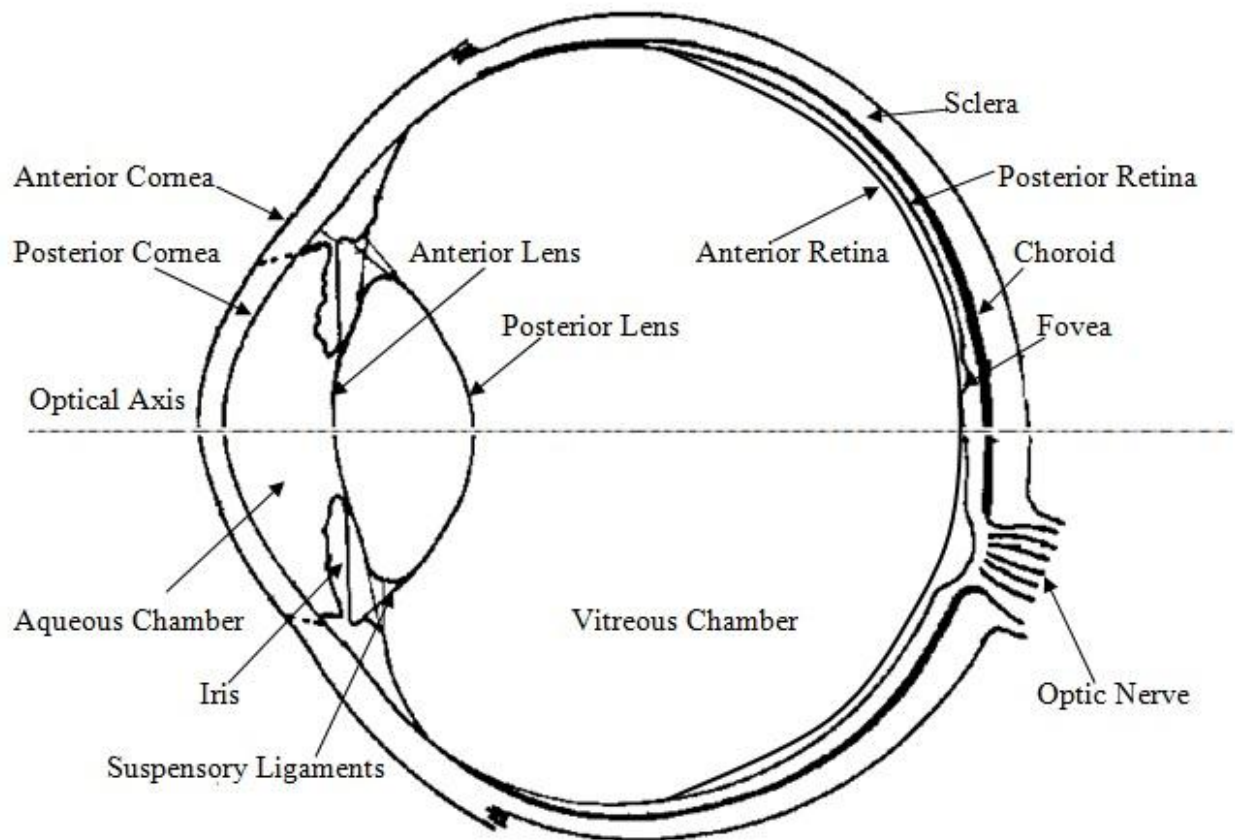


Figure 2.1: Schematic of a human eye consisting of different surfaces and other parts [40].

[Image taken from Optics of Human Eye by W.N. Charman and later edited]

2.2 Schematic of an eye

An eye is considered to be the most complex organ of a body where so many functions are performed by different parts of an eye in order to see an Image of an object. Talking about the vision the main parts of an eye that are responsible are cornea, lens and retina. In figure 2.1 we have mentioned anterior and posterior part of each layer. Anterior means the first part of layer and the posterior refers to the later part.

Cornea is the outer most and transparent part of an eye that contains iris, pupil and anterior chamber. Along with the help of anterior chamber and lens the light is refracted. Around

2/3 of the total refractive power is accounted by cornea. The radius of curvature of cornea is positive with variable thickness in different animal models. For an instance the corneal thickness of rat eye and radius of curvature of anterior cornea, reported by Chaudhuri et al [5] is $156\mu\text{m}$ and $3052\mu\text{m}$ respectively, whereas for mouse eye the thickness of cornea and radius of curvature is $93\mu\text{m}$ and $1517\mu\text{m}$ respectively as reported by Remtulla and Hallett [6]. Cornea has a refractive index which is higher than air, thus light coming from outside bends towards optical axis of an eye.

Generally speaking lens of an eye is biconvex crystalline structure by nature and is transparent to light. Lens has an ability to change the shape which accounts for change in the focal distance of the eye. This ability allows it to focus on distant objects. A real sharp image could be then realized at retina. Accommodation can be described as analogous to camera, where by adjusting the lens we can see distant object clearly. The Anterior lens is more flat than the posterior side of the lens. Anterior side has a positive radius of curvature whereas posterior side has negative radius of curvature.

Retina is the innermost light sensitive layer of the eye and is mostly build of layers of neurons. When the light falls on this layer, electrical and chemical events are initiated and nerve impulses are triggered. Optic nerves present next to retinal layer acts as a messenger and send the information to visual area of the brain. The visual cortex or visual part of the brain then processes the image and finally we are able to see the image. Likewise all the other surfaces have definite thickness, radii of curvature and refractive index so is the case of retina. Anterior as well as posterior retina has negative radius of curvature.

2.3 Modeling of an eye

In the preceding sections we have discussed different models of an eye and structure of an eye. Now we are ready to make a model that would appropriately draw all the 6 layers present in the eye. The most important part and beauty of the model lies in the fact that along with the schematic of an eye it also calculates the ocular parameters, i.e., radii of curvatures, centers of radii of curvatures, thicknesses of all the surfaces, averages of radii of curvatures, averages of depths of different chambers of eye. The above mentioned information is also written in a text file, all the images of plots are auto saved in the respective directory. The modeling of an eye is explained in a sequential manner as below.

2.3.1 Plot X-Y Coordinates

We were given ocular coordinates or X-Y coordinates of different layers of an eye in an excel sheet. Once we had defined the target eye to be plotted, the custom made program in MATLAB, will fetch the co-ordinate points from the respective excel sheet for each layer of an eye. For illustration table 2.1 below shows data (coordinates) for one of the layers that is present in the file. The specimen is M2_L taken from C57BL strain of mice. The data in table 2.1 represents the X-Y coordinates of posterior corneal layer.

If we carefully look at the data which is provided to us is humungous. There are total of 19 eyes of different mice strains and in each schematic of an eye we have 6 layers. In total we have 114 layers that need to be plotted. Each layer has at least 28 numbers of rows. In order to process such a large data we have come up with an algorithm, which automatically takes data of 6 layers for particular specimen of an eye and then plot the schematic of an eye based on that data.

No	Eye	X	Y
1	M2_L_TIF.tif	8868.6	4773.6
2	M2_L_TIF.tif	8798.4	4703.4
3	M2_L_TIF.tif	8704.8	4609.8
4	M2_L_TIF.tif	8611.2	4539.6
5	M2_L_TIF.tif	8494.2	4469.4
6	M2_L_TIF.tif	8353.8	4422.6
7	M2_L_TIF.tif	8190.0	4352.4
8	M2_L_TIF.tif	8073.0	4329.0
9	M2_L_TIF.tif	7932.6	4282.2
10	M2_L_TIF.tif	7815.6	4282.2
11	M2_L_TIF.tif	7698.6	4282.2
12	M2_L_TIF.tif	7558.2	4282.2
13	M2_L_TIF.tif	7464.6	4305.6
14	M2_L_TIF.tif	7371.0	4329.0
15	M2_L_TIF.tif	7254.0	4375.8
16	M2_L_TIF.tif	7137.0	4422.6
17	M2_L_TIF.tif	7020.0	4492.8
18	M2_L_TIF.tif	6926.4	4563.0
19	M2_L_TIF.tif	6832.8	4609.8
20	M2_L_TIF.tif	6786.0	4656.6
21	M2_L_TIF.tif	6739.2	4703.4
22	M2_L_TIF.tif	6669.0	4797.0
23	M2_L_TIF.tif	6598.8	4890.6
24	M2_L_TIF.tif	6528.6	5007.6
25	M2_L_TIF.tif	6481.8	5124.6
26	M2_L_TIF.tif	6435.0	5218.2
27	M2_L_TIF.tif	6388.2	5311.8

Table 2.1: X-Y coordinates of Posterior Corneal Layer of M2_L mice of C57BL.

Figure 2.2 shows the plotting of X-Y coordinates of 6 layers representing schematic of an eye. Also if we notice the plot is tilted as it is drawn as per the ocular coordinates and this could be accounted of the fact that the data extracted from MRI images could be in any orientation.

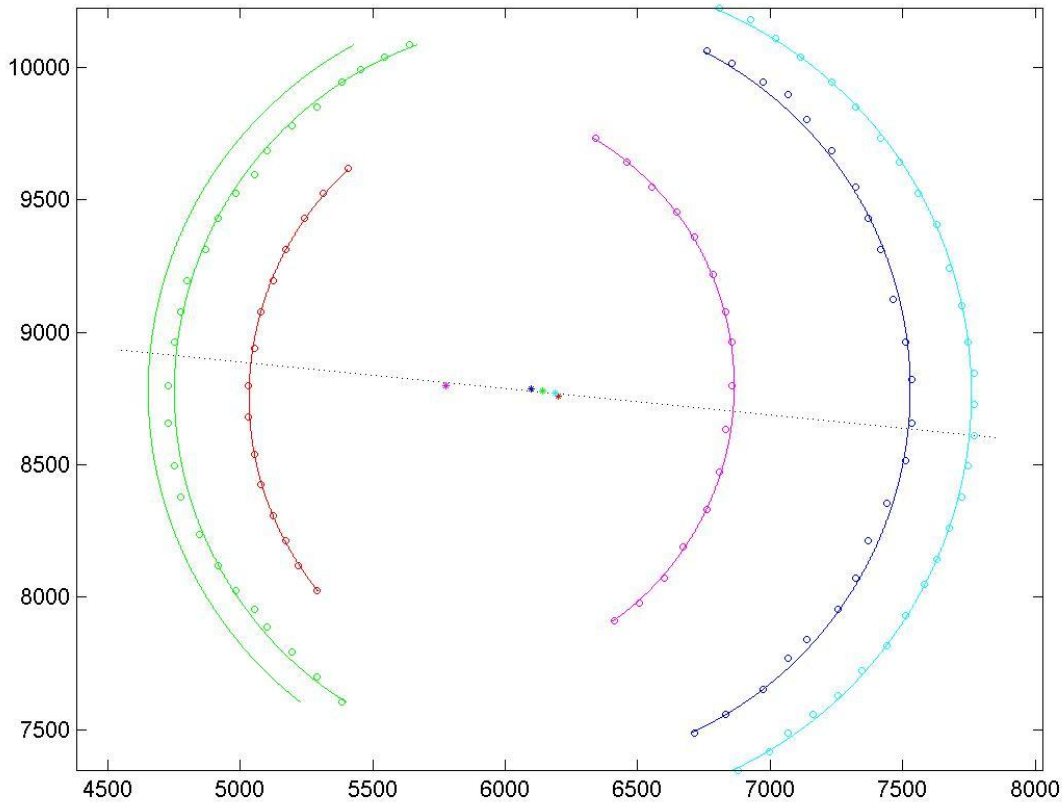


Figure 2.2: Schematic of an eye of #M1_L specimen of mice strain C57BL.

Along with the layers the small circular points on top of each layer represents the X-Y coordinates (raw points) of the respective layer. The first layer i.e., anterior cornea does not have any raw points, instead only thickness of the cornea is given to us. The raw points for the anterior cornea cannot be extracted because the outer layer is exposed to air and thus while taking MRI image the contrast ratio is very poor. The dotted line passing through the center of each layer is the optical axis of an eye.

We can see that image in figure 2.2 is disoriented and in order to change the orientation of the schematic, so that it looks like as if this is a virtual eye, we have to transform it from one co-ordinate to another. For that purpose we have calculated the angle by which it has to be shifted. After calculating the angle we have to estimate translation in terms of coordinates. Figure 2.3 shows an image of schematic of an eye after transformation. Also the first layer is at origin of the co-ordinate system i.e., coordinates of anterior cornea are (0, 0). The overall size of an eye is approximately $3000\mu\text{m}$.

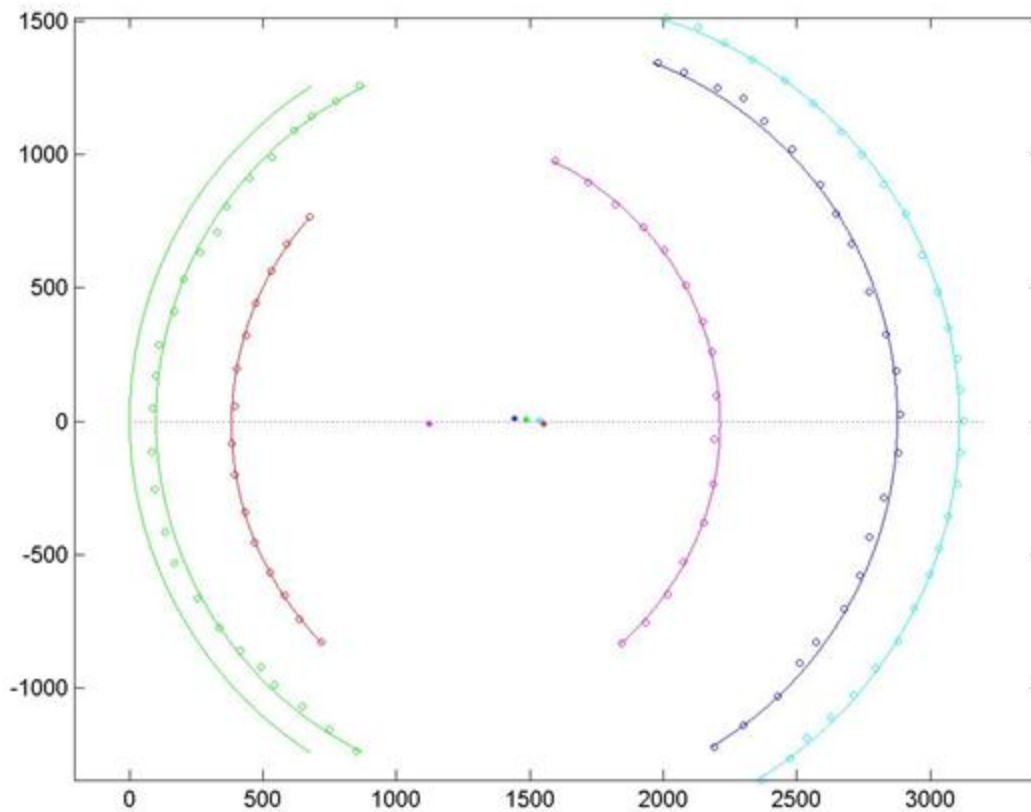


Figure 2.3: Image of an eye of #M1_L specimen of mice strain C57BL after transformation.

2.3.2 Smooth Curve Fitting

While plotting the schematics of an eye, in figure 2.3 we can see that some of the circular points are not lying exactly over the layer. The reason being, that we need maximum points to be

covered by the line and that two in curvy manner. In order to accomplish this task we followed least square regression approach. Linear regression is used to obtain best fit between the points.

2.3.3 Goodness of Curve

Least square fitting was used for plotting the raw data points. To verify how good the fit is we have calculated R^2 of arc. R^2 of arc returns a real value whose value is ≤ 1 . If the fitting of the curve is good its value comes out be very close to 1 approximately .99 and for bad curve fitting its value could fall way behind one. Eq. 2.1 shows the formula calculate R^2 of arc.

$$R^2 = 1 - \frac{SS_{err}}{SS_{tot}} \quad (2.1)$$

Where SS_{err} is Sum of Squares for error and is given by Eq. (2.2)

$$SS_{err} = (n - 1) \left(S_y^2 - \frac{S_{xy}^2}{S_x^2} \right) \quad (2.2)$$

S_y^2 , S_x^2 is variance of y and x respectively and S_{xy}^2 is covariance of x and y.

SS_{tot} is total sum of all the events of squared difference between each event from overall mean and is represented by Eq. (2.3)

$$SS_{tot} = \sum_{i=1}^n (Y_i - \bar{Y}_1)^2 \quad (2.3)$$

Where \bar{Y}_1 is the mean calculated over all values of Y_i .

2.3.4 Centers of Curvature, Radii and other Ocular Parameters

In preceding steps we have drawn the schematics of an eye, performed smooth curve fitting and then calculated R^2 of arc to find how good the fit is. The next step that would be required for the modeling of an eye and ray tracing in the proceeding chapters is calculation of radii of curvature, center of radii of curvature and distances between successive layers of an eye

(depths of different surfaces). All these steps are realized using different equations of geometry and mathematical calculation.

A) Center of curvature

We have number of points through which the line is passing resulting in an arc and using sophisticated code we had calculated center of curvature from all these points. But to better illustrate the process of calculation of center of curvature we are assuming three points as of now i.e. initial point (X_0, Y_0) , middle point $(X_{n/2}, Y_{n/2})$ and last point (X_n, Y_n) .

If we draw a normal from center of the curve of circle, then the point lying at the normal far away from the center of the curve is called as the center of curvature. In figure 2.4 point P_c is center of curvature. The approach below shows the calculation of center of curvature.

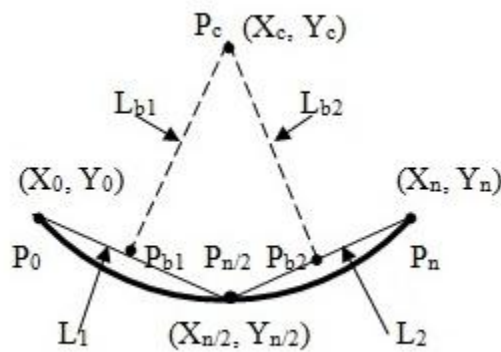


Figure 2.4: Arc from where co-ordinate points (X_c, Y_c) for center of radii of curvature are calculated using geometry.

First bisecting Point or midpoint P_{b1} through points (X_0, Y_0) and $(X_{n/2}, Y_{n/2})$ is given as

$$P_{b1} = \left(\frac{X_0 + X_{n/2}}{2}, \frac{Y_0 + Y_{n/2}}{2} \right) = (X_{b1}, Y_{b1}) \quad (2.4)$$

Second bisecting Point or midpoint P_{b2} through points $(X_{n/2}, Y_{n/2})$ and (X_n, Y_n) is given as

$$P_{b2} = \left(\frac{X_{n/2} + X_n}{2}, \frac{Y_{n/2} + Y_n}{2} \right) = (X_{b2}, Y_{b2}) \quad (2.5)$$

Slopes of lines L_1 and L_2 are represented by M_{L1} and M_{L2} is given by Eq. (2.6) and Eq. (2.7) respectively:

$$M_{L1} = \frac{Y_{n/2} - Y_0}{X_{n/2} - X_0} \quad (2.6)$$

$$M_{L2} = \frac{Y_n - Y_{n/2}}{X_n - X_{n/2}} \quad (2.7)$$

In order to calculate equations for lines or to plot lines L_{b1} and L_{b2} we would first find the slopes of the lines L_{b1} and L_{b2} which is inverse to the negative of slope M_{L1} and M_{L2} respectively. These slopes are represented by notation M_{Lb1} and M_{Lb2} and are given by Eq. (2.8) and Eq. (2.9) respectively:

$$M_{Lb1} = -\frac{1}{M_{L1}} = -\frac{X_{n/2} - X_0}{Y_{n/2} - Y_0} = \frac{X_0 - X_{n/2}}{Y_{n/2} - Y_0} \quad (2.8)$$

$$M_{Lb2} = -\frac{1}{M_{L2}} = -\frac{X_n - X_{n/2}}{Y_n - Y_{n/2}} = \frac{X_{n/2} - X_n}{Y_n - Y_{n/2}} \quad (2.9)$$

Once we have the slopes by using equation of line we can find center coordinates which are X-Y coordinates of curvature. In other we call it as center of curvature. Equation of lines for L_{b1} and L_{b2} are given by Eq. (2.10) and Eq. (2.11) respectively.

$$L_{b1}(X): Y = M_{Lb1}(X - X_{b1}) + Y_{b1} \quad (2.10)$$

$$L_{b2}(X): Y = M_{Lb2}(X - X_{b2}) + Y_{b2} \quad (2.11)$$

At $X = X_c$:

$$Y = M_{Lb1}(X_c - X_{b1}) + Y_{b1} = Y = M_{Lb2}(X_c - X_{b2}) + Y_{b2} \quad (2.12)$$

$$X_c(M_{Lb1} - M_{Lb2}) = -M_{Lb2}X_{b2} + Y_{b2} + M_{Lb1}X_{b1} - Y_{b1} \quad (2.13)$$

$$X_c = (M_{Lb1}X_{b1} - Y_{b1}) - (M_{Lb2}X_{b2} - Y_{b2}) / (M_{Lb1} - M_{Lb2}) \quad (2.14)$$

Thus Eq. (2.14) gives value for center of coordinates for X. Inserting values for X_c in Eq. (2.15) would give values for Y_c .

$$L_{b1}(X_c): Y_c = M_{Lb1}(X_c - X_{b1}) + Y_{b1} \quad (2.15)$$

B. Radius of Curvature

Radius of curvature is defined as the measurement of radius of the circular arc of curve, which defines the curve appropriately. If we know the locations of X-Y coordinates then we can calculate radius of curvature. Radius of curvature could be negative towards the concave side of lens and is positive towards the convex side of lens. Referring figure 2.4 and using mathematical equations of circle, we can find the radius of curvature as represented in Eq. (2.17).

Provided the X and Y coordinates equation of circle is given as:

$$R^2 = X^2 + Y^2 \quad (2.16)$$

$$R = \sqrt{X^2 + Y^2} \quad (2.17)$$

C. Depths of Surfaces

Depth of the surface or thickness of surface is defined as the distance between successive surfaces. Or we can say that depth is defined as the distance between locations, when the arc of first surface bisects the optical axis and the arc of second surface bisects the optical axis. For better illustration if we look at the figure 2.5 we have surfaces from S_0 to S_5 which corresponds to

6 layers of eye. Starting from first layer S_0 which represents first layer i.e., anterior cornea, distance between anterior cornea S_0 and posterior cornea S_1 is called as “Corneal Depth”. Similarly distance between S_1 (posterior cornea) and S_2 (anterior lens) is known as “Aqueous Chamber Depth”. If we keep on going like this the respective depths would be “Depth of Lens” or thickness of lens, “Vitreous Chamber Depth” and “Retinal Depth” or thickness of retina.

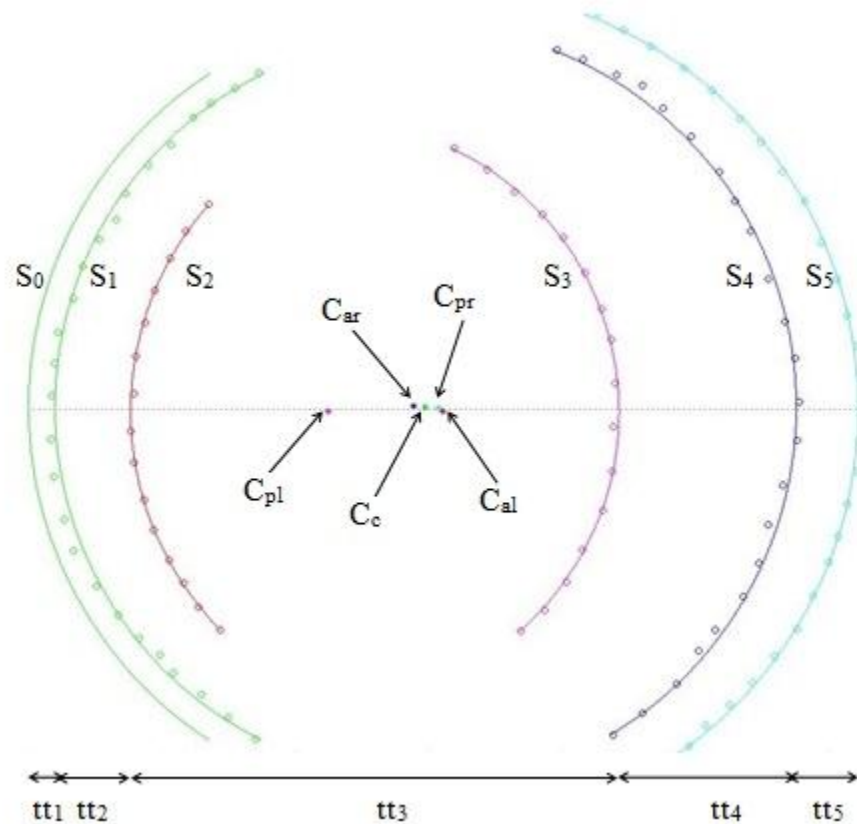


Figure 2.5: Schematic and Summary of an eye with ocular parameters. Surfaces are notated by letter S. $S_0, S_1, S_2, S_3, S_4, S_5$, are Surfaces of anterior cornea, posterior cornea, anterior lens, posterior lens, anterior retina and posterior retina respectively. Thickness or depths are represented by tt and $tt_1, tt_2, tt_3, tt_4, tt_5$ are thicknesses of cornea, aqueous chamber, lens, vitreous chamber and retina respectively. C represents center of curvature and is clear from subscript $C_c, C_{al}, C_{pl}, C_{ar}, C_{pr}$ and center of curvatures for cornea, anterior lens, posterior lens, anterior retina and posterior retina.

Note: We can see that there are no separate centers for anterior and posterior cornea because for anterior cornea we don't have ocular coordinates but just thickness that is provided to us.

Table 2.2 gives an overview and representation of all the ocular parameters that are calculated in the modeling of an eye.

Properties	NOTATIONS FOR SURFACES					
	Anterior Cornea	Posterior Cornea	Anterior Lens	Posterior Lens	Anterior Retina	Posterior Retina
Center of Curvature	C_c		C_{al}	C_{pl}	C_{ar}	C_{pr}
Radius of Curvature	r_{ac}	r_{pc}	r_{al}	r_{pl}	r_{ar}	r_{pr}
Surfaces	S_0	S_1	S_2	S_3	S_4	S_5
Thickness Or Depth	tt_1	tt_2	tt_3	tt_4	tt_5	
	$tt_1 = S_1 - S_0$	$tt_2 = S_2 - S_1$	$tt_3 = S_3 - S_2$	$tt_4 = S_4 - S_3$	$tt_5 = S_5 - S_4$	

Table 2.2: Summary of notations used in the model.

2.3.5 Average of Ocular Parameters

Meanwhile geometry of an eye has been built for each specimen of mice strain using mathematical approach, the next step to be performed is average of all ocular data for each strain over all specimen of an eye. This step is incited by the fact that there are different numbers of specimens for same strain of mice for which the schematics are plotted and we can average all the data and can plot one eye for single strain. Thus averages of radii of curvatures, centers of curvatures and depths of the surfaces are calculated.

Average over any set of numbers ($n_1, n_2 \dots n_i$) is given as sum of values of all numbers ($n_1 + n_2 + \dots + n_i$) in a set divided by the total number present (m) and is given by Eq. (2.18)

$$\text{Average} = \frac{1}{m} \sum_{i=1}^m n_i \quad (2.18)$$

As an example we can take first strain (C57BL) of mice where we have 6 specimen of eye and the layer for which we would elaborate the concept of average for ocular surfaces is “Anterior Cornea”.

The radius of curvature of anterior cornea r_{ac} averaged over all specimen of the first strain of mice can be expressed as shown in Eq. (2.19) and Eq. (2.20)

$$\text{Average } (r_{ac}) = \frac{r_{ac1} + r_{ac2} + r_{ac3} + r_{ac4} + r_{ac5} + r_{ac6}}{6} \quad (2.19)$$

$$\text{Average } (r_{ac}) = \frac{1}{6} \sum_{i=1}^6 r_{aci} \quad (2.20)$$

Similarly we can obtain radius of curvatures for other 5 surfaces viz. viz. r_{pc} , r_{al} , r_{pl} , r_{ar} and r_{pr} for posterior cornea, anterior lens, posterior lens, anterior retina and posterior retina respectively.

Thickness of Surface of Anterior cornea is averaged over all eyes of the single strain of mice and is represented as shown in Eq. (2.21) and Eq. (2.22)

$$\text{Average } (tt_1) = \frac{tt_1 + tt_2 + tt_3 + tt_4 + tt_5}{5} \quad (2.21)$$

$$\text{Average } (tt_1) = \frac{1}{5} \sum_{i=1}^5 tt_i \quad (2.22)$$

Same approach is followed for centers of curvatures and $C_c (X_i, Y_i)$ is given as:

$$\text{Average } (C_{c1}) = \frac{C_{c1} + C_{c2} + C_{c3} + C_{c4} + C_{c5}}{5} \quad (2.21)$$

$$\text{Average } (C_{c1}) = \frac{1}{5} \sum_{i=1}^5 C_{ci} \quad (2.22)$$

2.3.6 Average Schematic of an Eye

Since all the ocular parameters have been averaged over all specimens of single strain, we can also draw a single schematic of an eye of one strain. Figure 2.6 below shows one schematic of strain C57BL averaged over all the eyes of those specimens.

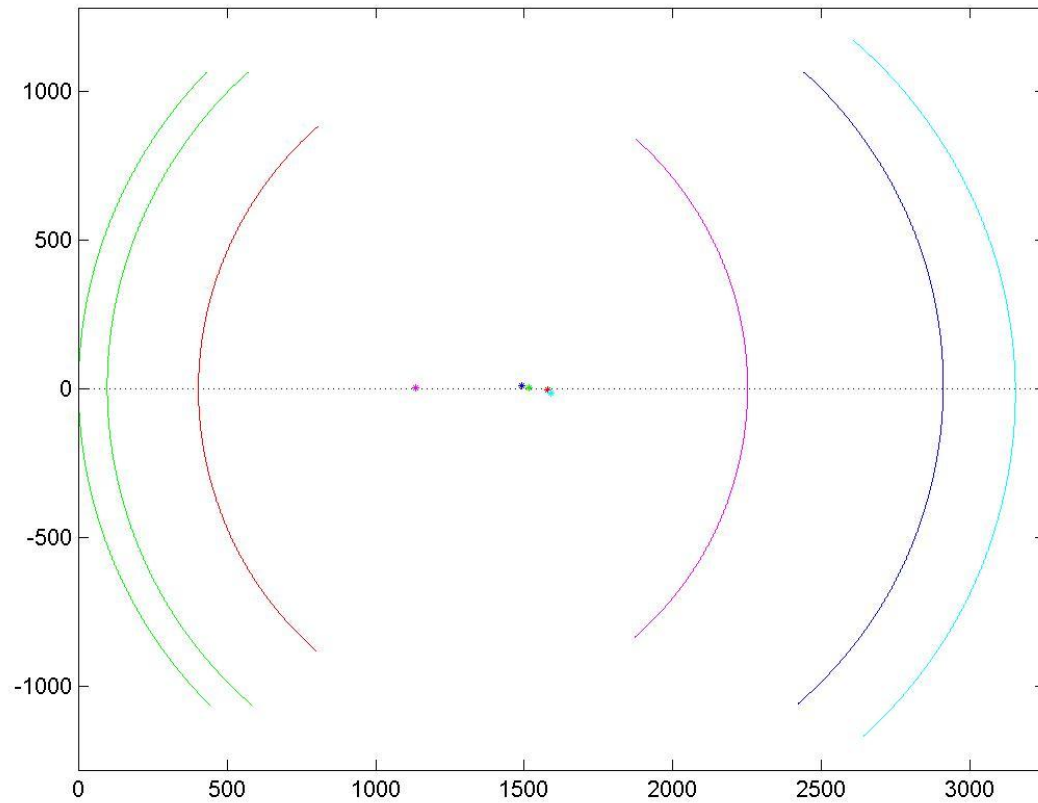


Figure 2.6: Schematic of an eye of C57BL mice strain drawn as a result of all the ocular parameters averaged over all 6 specimens of the same strain.

CHAPTER 3

IMAGE PROCESSING

Image processing may be defined as the process in which an image is input and output of an image could be in an image itself or data in terms of numbers representing an image. In most of the cases image is a 2 dimensional containing data as rows and columns and image processing is considered as processing of data in two dimensions. In real world an image can be represented as $M(X, Y)$. M is the amplitude of the quantity which is a function of the variables, X and Y co-ordinates. The techniques involved in processing of an image are similar as if we have two dimensional signals in a space.

Image processing in our work is done in terms of superimposing two images. The first image is schematics of an eye obtained as a result of modeling of eye which is explained in the previous chapter, and the second image is the MRI image of an eye from where the ocular parameters (X - Y Co-ordinates) were extracted. We can say that there should not be much difference in two images as the former is a result of the second image as schematic is drawn from the co-ordinates of MRI image. We have superimposed two images to visually analyze if the layers of both the images are coinciding with each other.

Many algorithms have been proposed till now for image processing and in particular when talking of images having boundaries, as in the case of schematic of an eye that contains different layers, edge detection [37, 38, 39] is appropriate way of solving the problem. First and the foremost step is to find the Region of Interest (ROI) to be processed in whole object. After the boundary of the object is detected, extract the information and then process the extracted information. Processing of the extracted information could imply that the boundary of the image is achieving certain target set forth in user defined problem.

In our case we have used simple concepts of image processing instead of edge detection algorithms to trivialize the problem of overlapping two images. Due to certain limitations of available resources we have decided not to approach the problem using complex edge detection algorithms. The primary reason was that MRI images of the samples do not have very well defined sharp boundaries and the contrast ratio is also very low. Secondly for overlapping of two images to get composite image (MRI and generated schematics of an eye with different layers), that is bound to yield a secondary confirmation of the correctness of the approach that we have followed, we can simply redraw the plots on the original image, of course with the help of sophisticated algorithm and bypassing the use of many complex algorithm for the same. The algorithm written by us is converting the MRI images into RGB and image for schematic of an eye consisting of 6 layers, drawn from raw points is binary.

Formation of composite image or overlapping of an image is performed with the help of a program that is written in MATLAB. It takes the MRI image of the targeted eye of mice strain then it looks for the targeted image that is created by modeling of an eye. After loading the images, program uses the MRI image as a background and plots the layers of the schematic of the model that we built. The process of Image processing was executed step by step in the following manner.

3.1 Locate the images

The MRI images of all the specimens of every strain are given to us by School of Medicine, Detroit, for the comparison with the images of schematic of an eye generated by us. The program written would map both the images or in other words we can say that program would locate the images which are present in their respective folders. For an example if we want

to compare the image of schematic of eye #M1_L of C57BL strain it would first scan for the directory where our model has auto saved all the images of schematic and tag it. Then it would move on to other directory where our MRI images are present and would locate and tag the targeted schematic of an eye.

3.2 Rotation of MRI image and overlapping of two Images

In the previous chapter we have explained the schematic of an eye was disoriented as it was not normal to an eye and for correct orientation we have to apply an algorithm. Images of MRI confirm the claim as we can see them.

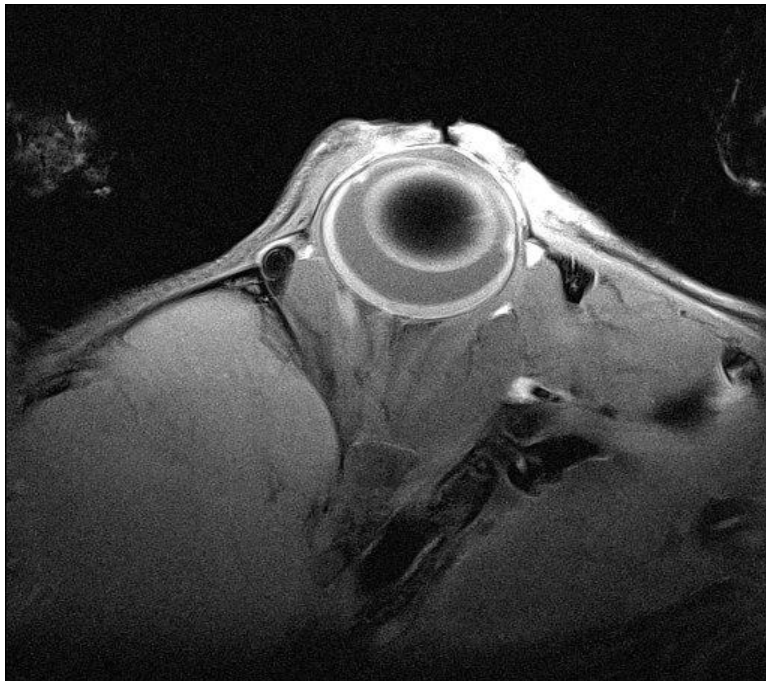


Figure 3.1: The MRI image of an eye. Along with the eye ball other surrounding tissues and blood vessels are also visible.

One of the images is shown in figure 3.1 where we can see that aperture of an eye faces upside and we have to rotate the image by certain degree in order to imagine the eye as is

discussed in literature. We can clearly see the six layers of an eye i.e., anterior cornea, posterior cornea, anterior lens, posterior lens, anterior retina and posterior retina, which we had defined earlier. After rotating the MRI image by 90 degrees the aperture of an eye is on the left side as shown in figure 3.2. We can say that light is entering into eye having an optical axis and the ray is originated from x-axis. However for proper orientation there is need of co-ordinate shifting.

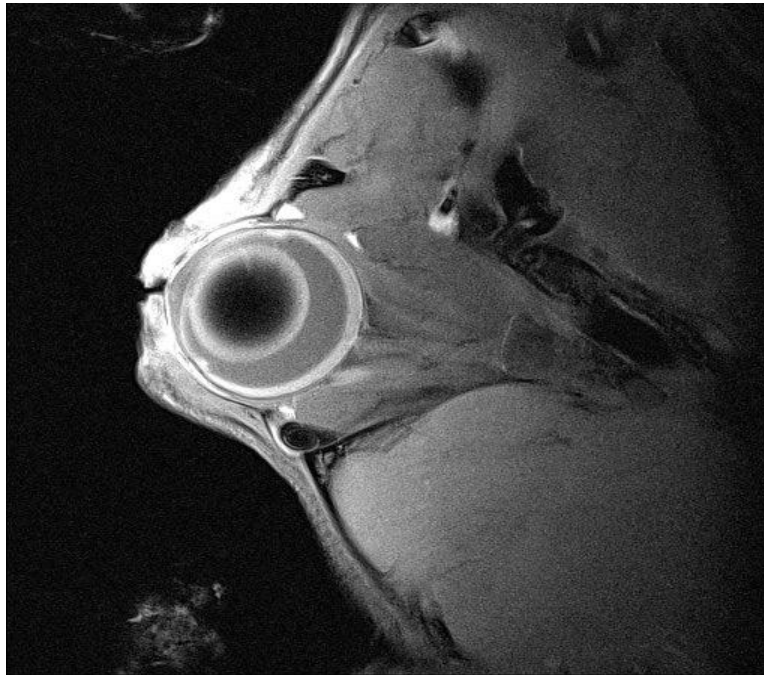


Figure 3.2: Image after rotating 90 degrees to the left.

As we have all the algorithms present to generate a smooth curve across the raw points the only thing that we are concerned is plotting the layers directly over MRI image. Before we can perform this step few challenges has to be met.

1. The pixels size of MRI images and pixels of the images of schematic of an eye, which are generated by our model, are different. Dimensions of MRI images are 512 x 512 and images of

schematics of an eye are 1200 x 900. We have to match the pixel size to get the sense of superimposed image, which is a composite of two images, and also the layers that need to be plotted on MRI image exactly overlays. In order to accomplish this we have to shrink the size of an image to 512 x 512 so that plots of the schematics are 512 pixels and are thus lying exactly at the location where we have the eye ball as shown in figure 3.2.

2. After shrinking the size we would construct the schematic of an eye layer by layer. Figure 3.3 shows different layers of an eye.

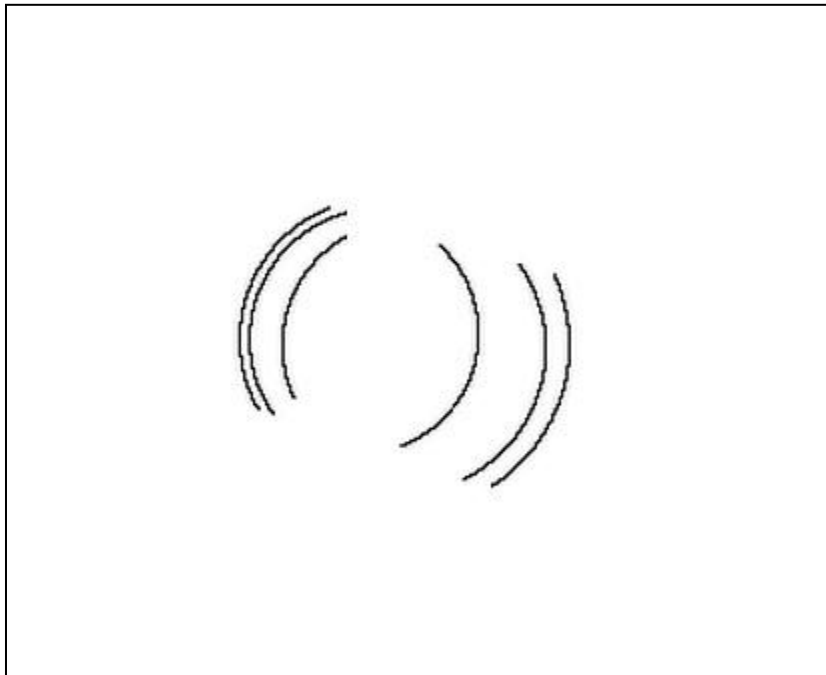


Figure 3.3: Different plotted layers of an eye.

3. Now we have the layers of an eye present and pixels size is also adjusted in such a way that both the images as shown in figures 3.2 and 3.3 are of same dimensions. The next step is to overlap both the images. Figure 3.4 shows the resulting image which is a composite of two

images and are superimposed on each other. The red layers represent all the 6 layers of an eye that has been discussed earlier and the background image is MRI image of an eye.



Figure 3.4: Overlapping of MRI image and layers drawn from the raw points. MRI image served as background and layers drawn in red are on top of that.

4. In the image shown in figure 3.4, red layers lying over the MRI image, gives us an idea about the accuracy of our model. Also in image we can see that volume occupied by an eye ball is very less and surrounding area is covered with tissues, vessels, neurons and other essential parts. Thus region of interest (ROI) is very small and we need to somehow zoom in to see the images to visually analyze. It can be done in two ways we can zoom in manually and observe it or otherwise we can use two variables which would define the aperture of an eye and then accordingly the layers would be drawn with the pre-defined aperture. For example if the aperture

size is 2000 μm then our program will draw the layers with Y co-ordinates as 1000 μm above and -1000 below the optical axis. Y co-ordinates define the aperture size or the height of an eye ball through which light will enter the eye ball. The resulting image is shown in figure 3.5 where we can see that ROI excluding all other parts of an eye.

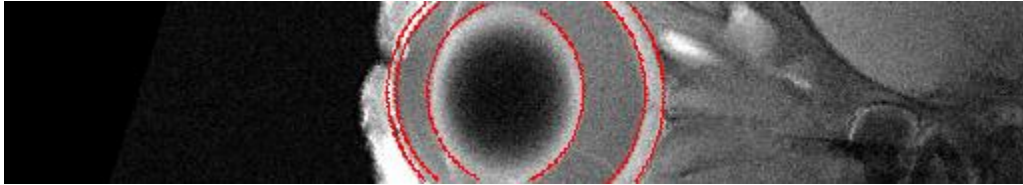


Figure 3.5: Composite image of Region of interest in an eye.

3.3 Visual Analysis

Besides the low contrast ratio and other limitations we were able to build a composite image that is giving us an idea of accuracy of the modeling. We have the final image where we can analyze how good the modeling of an eye is. In figure 3.5 we can see that layers shown in red colors are exactly lying over the respective layers of an eye in MRI image. There is a part of an eye at the edges where the layer of an eye are not perfectly aligned which could be accounted for the reason that while extracting the raw points from the MRI images there could be possible error. The other reason could be that the least square regression line is not exactly taking the points and is drawing the line in neighborhood for good overall fit of the curve around the respective layers. But the claim of our correct approach is evident by the fact that while modeling of an eye we have calculated the statistical quantity, R^2 of arc. Closer the value of R^2 of arc to 1 better the curve fitting is and in our case for all the specimens of all 4 mice strains for all the layers the number is varying from 0.995 to 0.999.

CHAPTER 4

OPTICAL MODELING AND RAY TRACING

Ray optics which is a better name to be called upon instead of geometric optics is associated with the light ray. However as such entity “Ray” does not exist but it can be realized using the fundamentals of geometry which explains the formation of lines along the paths in which light is perceived. The concept of rays work in some cases but it fails in others situations, such as quantum physics, electromagnetic waves etc. With the help of corpuscular and wave theory rays have been defined. In corpuscular theory we talk of path of corpuscles and photons. But the difficult situation arises when energy densities approaches to infinity. In wave theory also the efforts are put forth to define rays as quantities which are associated with wave theory both as scalar as well as electromagnetic. Rays are tried to be explained as wavefront normal, pointing vectors, description of wave behavior in high frequency limit [41], quantum mechanical model [42], a discontinuity in electromagnetic field [43, 44].

In above models where we have tried to define rays, there are always some problems associate alongside, as there are many cases where vectors and wavefronts become too complicated or meaningless. One of the cases of such complications can be explained as interference of two coherent plane waves, where there is no sharp well defined region of wavefront at overlapping regions. In order to avoid the complications as a consequence of these models we would treat the tracing of rays as a mathematical model where the formations of rays is explained by using concepts of geometry and rays are simply lines arrived from equation of lines.

Geometric optics makes use of some other quantities such as refractive indices of surfaces along with other assumptions. Other assumptions could be properties of the surfaces,

such as spherical or aspherical and chromatic aberrations etc. Here we are limited to the modeling of an eye and we assume the surfaces are spherical. Also we would involve those parameters that are associated with the biconvex nature of the lenses. Those parameters are related to curvatures of lenses such as radius of curvatures of surfaces, thicknesses of surfaces and centers of radii of curvatures. Based on those assumptions we can say that we are going to build a ray tracing model in paraxial approximation in which the light would travel through different surfaces of the eye. The surfaces have positive as well as negative radii of curvatures as is typical in case of biconvex lenses.

The light rays that are traveling along the optical axis of eye, would go through the phenomenon of refraction as well as reflection which is an ideal situation in optics. Along with the refraction there would be bending of light towards or away from the optical axis as the medium of the eye is not uniform. Talking of medium it specifies different refractive indices that are inherent properties of an eye. If we see one of the images of the eye we would see different cavities in the eyes and those cavities are filled with liquid which has certain refractive indices. This liquid filled in cavity is called as medium. Further following principles of Snell's law [42, 43] and equations of geometry the light rays travel the distance. Finally those rays converge at one point in an eye which is photoreceptive part of the eye and lies at retina.

We can hence summarize this paraxial ray tracing as cone of light rays that are emanated from source ($x = -\infty$) and are traveling along the optical axis, enters through pupil into eye and passes through first two layers of an eye which are anterior and posterior cornea respectively. In conjunction with refractive index of cornea and aqueous chamber the rays refract to lens surface. The lens having two parts, anterior as well as posterior, and is filled with refractive index of medium along with the vitreous chamber (cavity between posterior lens and anterior retina)

focuses the rays at retina. Retina is the photoreceptive part of an eye which consists of neurons also has refractive index of medium and contributes in focusing of the light beams. The light beams when falls on the photoreceptive part, consisting of neurons, gets activated and sends signals to visual cortex of brain. This area then processes the information and we can see the image finally. In this image formation also other parameters are involved which are discussed later.

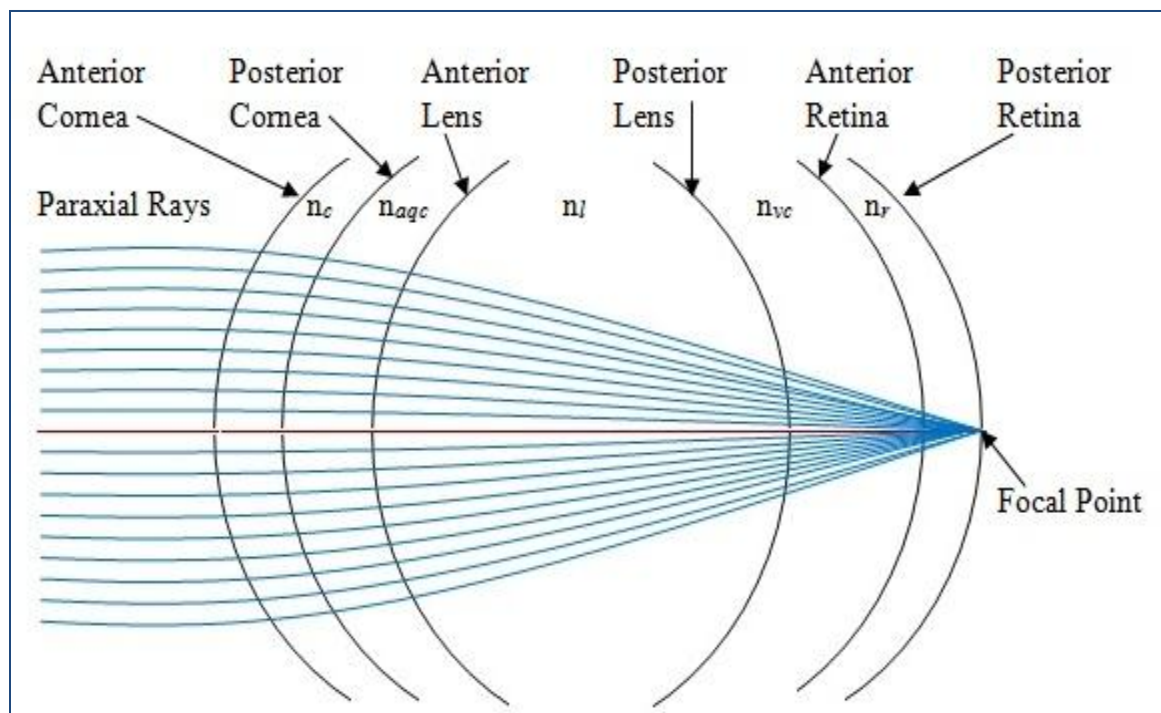


Figure 4.1: Schematic of an eye with different layers and their respective refractive indices.

[Note: In above figure very few lines, before the first interface look not parallel to optical axis, because of limitation of drawing tools we have. But this is just an illustration and in real paraxial model rays model as shown in figure 4.2 rays are always travelling parallel to optic axis until the first interface]

Figure 4.1 shows all the layers present in an eye from outer side to inner side of eye. These layers are acting as lenses having curvatures and with the help of refractive indices the

rays are bending as well as refracting at successive boundaries of the eye and finally converging at one final point which is called as focal point.

4.1 Computational Model for Ray tracing

We have discussed above the different theories of defining the ray and the simplest approach of defining the ray tracing method. Also we have discussed how the rays enter through an eye and after the phenomenon of refraction light travels through different surfaces and finally meet at a point known as a focal point. Above described model was an approximation of how the ideal case behaves. Talking of idealism means that all the parameters are adjusted in such a way that there is a sharp point at the retina i.e., photoreceptive part and hence a sharp image that we see after processing of information that is passed from the photoreceptive area to the visual cortex of the brain.

We are studying the behavior of the mouse eye here, thus in order to do ray tracing we should have all the parameters which are essential for the ray tracing. Those parameters are Radius of curvatures (r), Thicknesses or depths of surfaces, which we have already calculated while doing modeling of an eye, along with Refractive indices of media. These ocular parameters inserted in the equation for lines, which are described in the later part, explain the paraxial model as well as ocular ametropia or refractive error of an eye.

4.1.1 Ocular Parameters of Mouse and Rat eye:

Schematics as well as ocular parameters of rat and mouse eye have been given by many researchers. Hughes [3], Campbell and Hughes [4] and Chaudhuri et al [5] worked on rat schematics using ocular parameters reported in table 4.1. Remtulla and Hallett [6] and Schmucker and Schaeffel [7] worked towards schematic of mouse eye using ocular parameters

reported in table 4.2. The refractive indices were measured at different wavelengths. These ocular parameters would be used for the ray tracing, discussed in the upcoming section, and eventually ray tracing would lead us to find the refractive errors of an eye.

Parameters	Anterior Cornea	Posterior Cornea	Anterior Lens	Posterior Lens	Anterior Retina	Posterior Retina
Radius (r, μm)	3051 (r_{ac})	2959 (r_{pc})	2535 (r_{al})	-2441 (r_{pl})	-3543 (r_{ar})	-3706 (r_{pr})
Thickness (tt, μm)						
	156 (tt_c)	708 (tt_{aqc})	3814 (tt_l)	1409 (tt_{vc})	217 (tt_r)	
Refractive Index (n) at Wavelength (nm)	n_c	n_{aqc}	n_l	n_{vc}	n_r	
$\lambda = 475$	1.3882	1.3381	1.6974	1.3379	1.3379	
$\lambda = 500$	1.3864	1.3366	1.6925	1.3367	1.3367	
$\lambda = 525$	1.3848	1.3355	1.6888	1.3358	1.3358	
$\lambda = 550$	1.3838	1.3346	1.6854	1.3349	1.3349	
$\lambda = 575$	1.3829	1.3336	1.6825	1.3341	1.3341	
$\lambda = 600$	1.3821	1.3329	1.6798	1.3332	1.3332	
$\lambda = 625$	1.3812	1.3321	1.6777	1.3322	1.3322	
$\lambda = 650$	1.3804	1.3315	1.6761	1.3319	1.3319	

Table 4.1: Summary of Ocular parameters of rat Eye. Values of Refractive indices are taken at wavelengths ranging from 475nm to 650nm with regular interval of 25nm.

Parameters	Anterior Cornea	Posterior Cornea	Anterior Lens	Posterior Lens	Anterior Retina	Posterior Retina
Radius (r, μm)	1517 (r_{ac})	1463 (r_{pc})	1248 (r_{al})	-1155 (r_{pl})	-1643 (r_{ar})	-1666 (r_{pr})
Thickness (tt, μm)						
	93 (tt_c)	452 (tt_{aqc})	2032 (tt_l)	558 (tt_{vc})	237 (tt_r)	
Refractive Index (n) at Wavelength (nm)	n_c	n_{aqc}	n_l	n_{vc}	n_r	
$\lambda = 488$	1.4102	1.3390	1.6952	1.3390	1.3390	
$\lambda = 544$	1.4060	1.3376	1.6778	1.3365	1.3365	
$\lambda = 596$	1.4030	1.3353	1.6665	1.3343	1.3343	
$\lambda = 655$	1.4015	1.3336	1.6590	1.3329	1.3329	

Table 4.2: Summary of Ocular parameters of mouse Eye. Values of Refractive indices are taken at wavelengths 488nm, 544nm, 596nm and 655nm.

In our case as mentioned earlier we have worked on 4 different strains of mice having number of specimens. Similar tables consisting of ocular parameters of mice eyes for all the strains averaged over all specimen of each single strain that were calculated while modeling of an eye are also shown in table 4.3, table 4.4, table 4.5 and table 4.6. Refractive indices are taken at two different wavelengths 500nm and 510nm.

Parameters	Anterior Cornea	Posterior Cornea	Anterior Lens	Posterior Lens	Anterior Retina	Posterior Retina
Radius (r , μm)	1507 (r_{ac})	1410 (r_{pc})	1171 (r_{al})	-1119 (r_{pl})	-1390 (r_{ar})	-1550 (r_{pr})
Thickness (tt , μm)	$\underbrace{\hspace{1.5cm}}$ 97 (tt_c)	$\underbrace{\hspace{1.5cm}}$ 308 (tt_{aqc})	$\underbrace{\hspace{1.5cm}}$ 1849 (tt_l)	$\underbrace{\hspace{1.5cm}}$ 659 (tt_{vc})	$\underbrace{\hspace{1.5cm}}$ 239 (tt_r)	
Refractive Index (n) at Wavelength (nm)	n_c	n_{aqc}	n_l	n_{vc}	n_r	
$\lambda = 500$	1.4094	1.3387	1.6917	1.3387	1.3500	
$\lambda = 510$	1.4085	1.3383	1.6880	1.3378	1.3500	

Table 4.3: Summary of ocular parameters of C57BL mouse strain averaged over all specimens

Parameters	Anterior Cornea	Posterior Cornea	Anterior Lens	Posterior Lens	Anterior Retina	Posterior Retina
Radius (r , μm)	1532 (r_{ac})	1431 (r_{pc})	1144 (r_{al})	-1141 (r_{pl})	-1438 (r_{ar})	-1605 (r_{pr})
Thickness (tt , μm)	$\underbrace{\hspace{1.5cm}}$ 101 (tt_c)	$\underbrace{\hspace{1.5cm}}$ 309 (tt_{aqc})	$\underbrace{\hspace{1.5cm}}$ 1831 (tt_l)	$\underbrace{\hspace{1.5cm}}$ 706 (tt_{vc})	$\underbrace{\hspace{1.5cm}}$ 233 (tt_r)	
Refractive Index (n) at Wavelength (nm)	n_c	n_{aqc}	n_l	n_{vc}	n_r	
$\lambda = 500$	1.4094	1.3387	1.6917	1.3387	1.3500	
$\lambda = 510$	1.4085	1.3383	1.6880	1.3378	1.3500	

Table 4.4: Summary of ocular parameters of C57L mouse strain averaged over all specimens






Parameters	Anterior Cornea	Posterior Cornea	Anterior Lens	Posterior Lens	Anterior Retina	Posterior Retina
Radius (r , μm)	1429 (r_{ac})	1318 (r_{pc})	1200 (r_{al})	-1137 (r_{pl})	-1383 (r_{ar})	-1609 (r_{pr})
Thickness (tt , μm)	 111 (tt_c)	 306 (tt_{aqc})	 1870 (tt_l)	 593 (tt_{vc})	 239 (tt_r)	
Refractive Index (n) at Wavelength (nm)	n_c	n_{aqc}	n_l	n_{vc}	n_r	
$\lambda = 500$	1.4094	1.3387	1.6917	1.3387	1.3500	
$\lambda = 510$	1.4085	1.3383	1.6880	1.3378	1.3500	

Table 4.5: Summary of ocular parameters of CE mouse strain averaged over all specimens





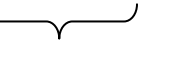
Parameters	Anterior Cornea	Posterior Cornea	Anterior Lens	Posterior Lens	Anterior Retina	Posterior Retina
Radius (r , μm)	1370 (r_{ac})	1268 (r_{pc})	1172 (r_{al})	-1083 (r_{pl})	-1497 (r_{ar})	-1677 (r_{pr})
Thickness (tt , μm)	 102 (tt_c)	 267 (tt_{aqc})	 1793 (tt_l)	 524 (tt_{vc})	 218 (tt_r)	
Refractive Index (n) at Wavelength (nm)	n_c	n_{aqc}	n_l	n_{vc}	n_r	
$\lambda = 500$	1.4094	1.3387	1.6917	1.3387	1.3500	
$\lambda = 510$	1.4085	1.3383	1.6880	1.3378	1.3500	

Table 4.6: Summary of ocular parameters of CZECH mouse strain averaged over all specimens

Since we have all the parameters that are required for the ray tracing we can now incorporate all those parameters in ray tracing formulae. We have worked on paraxial ray model which is characteristic of the incident rays that are coming parallel to the optical axis and the height of those rays is very small.

4.1.2 Ray Tracing

Ray tracing for both animal models rat as well as mouse eyes has been accomplished by making use of laws, fundamentals and principles of paraxial optics [44] and a custom computer program written and run in MATLAB[®] (The MathWorks, Inc., Natick, MA). Snell's law [45, 46] and principles of optics were applied to obtain ray paths and the optical geometry of eye. The forthcoming ray tracing model has been described is a result of exact formulae for Snell's law applied at every interface, and thus it is acceptable for wide-angle ray tracing as well. In our work, the subject of study is restricted to analysis of paraxial ocular parameters, more precisely the ametropia and its dependence on the radii of curvature, relative distances, and refractive indices of the eye components.

As is the requirement of the model and particular numerical implementation, the input ray that approaches the eye is parallel to the optical axis, and height of the ray from optical axis, y_p , is set very small as compared to all the linear dimensions of the ocular components. With the help of program written in MATLAB, we have observed that with $y_p < 25\mu\text{m}$, the exact ray tracing model begets the values for ametropia, as well as locations of all cardinal points, consistent with the models reported in [5-7].

The parameters that are used for ray tracing model are radii of curvatures, thickness of ocular components and refractive indices of the ocular refractive media. Fig. 4.2 shows main

refracting surfaces, ocular components and paraxial schematic model of the emmetropic rodent eye. For the emmetropic eye, which has zero refractive error (ametropia, A), paraxial rays of light traveling parallel to the optical axis will converge at the focal point located at the photoreceptor layer of the retina. In the case of the myopic eye ($A < 0$), the focal point will be located in front of the retina, whereas in the case of the hyperopic eye ($A > 0$), the focal point will be located behind the retina.

Paraxial rays that emanates from the source located at $x = -\infty$, refracts through different surfaces converges at a particular point, which is defined as the back focal point. The corresponding plane to back focal point is known as the back focal plane (Bf). Similarly if the source is located at $x = +\infty$ and the paraxial rays after number of refractions through surfaces, meet at a point in front of surfaces is called as front focal point and the plane corresponding to it is front focal plane (Ff). When the rays from front and back focal points are back-traced and the incident rays travel without changing their angles, the incident rays and focal point rays will intersect at specific points. These points of intersection are called front principal and back principal points respectively. The planes corresponding to the front and back principal points are called front principal plane (Fp) and back principal plane (Bp). Nodal Points are points of unit angular magnification. Paraxial ray that is entering object space at nodal point appears to leave the image space at different point. The planes corresponding to that are called as nodal planes (Fn for front nodal point and Bn for Back nodal points). Fig. 4.2 shows all layers and planes with the proper notations.

All the ocular parameters, i.e., radii of curvature (r), thicknesses of ocular components (tt), and refractive indices of ocular media (n), to perform ray tracing are written in the vector form as below:

$$\mathbf{r} = [r_{ac}, r_{pc}, r_{al}, r_{pl}, r_{ar}, r_{pr}]; \quad \mathbf{tt} = [tt_c, tt_{aqc}, tt_l, tt_{vc}, tt_r]; \quad \mathbf{s} = [s_1, s_2, s_3, s_4, s_5, s_6];$$

$$\mathbf{n} = [n_c, n_{aqc}, n_l, n_{vc}, n_r];$$

where s denotes the points in which layers intersect the x plane or, thus, denoting the location of the layers on the x -axis. Elements of s can be written as:

$$s_1 = 0; \quad s_2 = tt_c; \quad s_3 = tt_c + tt_{aqc}; \quad s_4 = tt_c + tt_{aqc} + tt_l; \quad s_5 = tt_c + tt_{aqc} + tt_l + tt_{vc};$$

$$s_6 = tt_c + tt_{aqc} + tt_l + tt_{vc} + tt_r$$

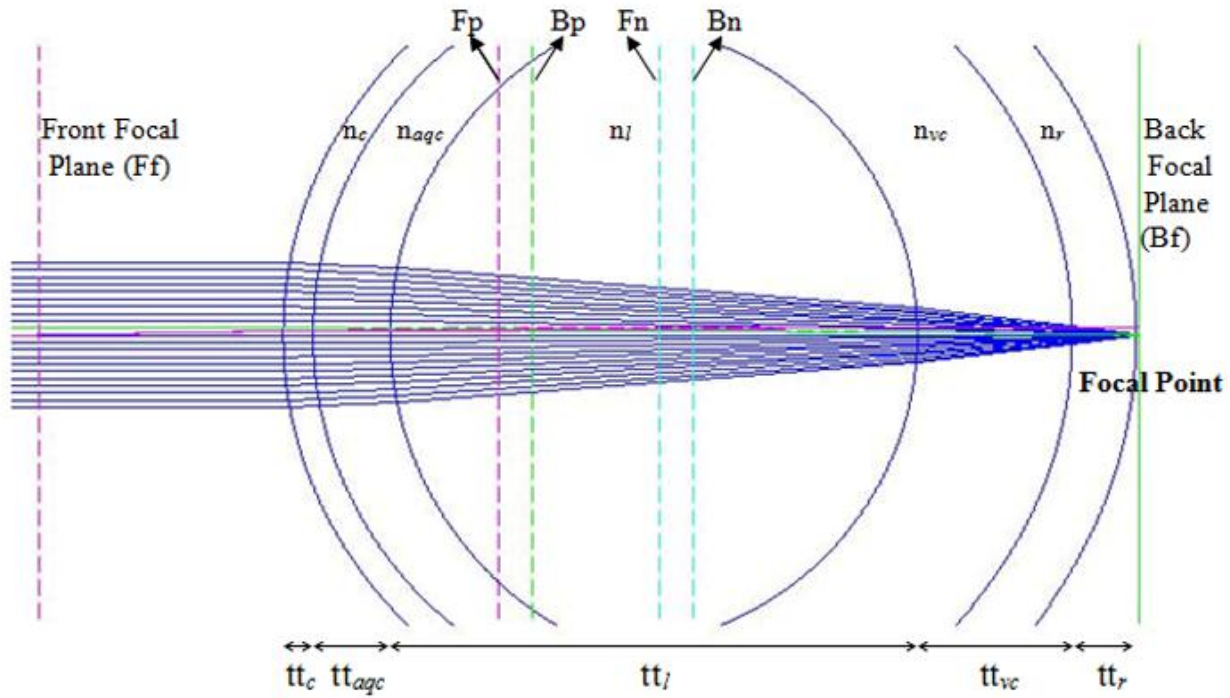


Figure 4.2: Paraxial schematic model of emmetropic rodent eye.

Paraxial rays meet at the focal point located at the level of photoreceptors. The eye consists of six main refracting surfaces, i.e., anterior cornea, posterior cornea, anterior lens, posterior lens,

anterior retina, and posterior retina. The main volume of a rodent eye is occupied by the crystalline lens, followed by the vitreous chamber, anterior chamber, and retina respectively. Fp: front principal plane; Bp: back principal plane; Ff: front focal plane; Bf: back focal plane; Fn: front nodal point; Bn: back nodal point; n_c : refractive index of cornea; n_{aqc} : refractive index of the aqueous; n_l : refractive index of the lens; n_{vc} : refractive index of the vitreous; n_r : refractive index of the retina; t_c : thickness of the cornea; t_{aqc} : anterior chamber depth; t_l : thickness of the lens; t_{vc} : vitreous chamber depth; t_r : thickness of the retina.

Since we have all the necessary elements that are required in order to derive the equations of rays as well as ray tracing and eventually would allow us to do the analysis, the next thing is to work on ray tracing itself. For forward ray tracing paraxial rays are coming from infinite source, thus $x_0 = -\infty$ and height of paraxial rays (y_p) is $y_0 = y_p$. Slope is given as $t_0 = -(y_0/x_0)$. Further for the modeling $X_{\min} = 0$ and $X_{\max} = \text{length of surfaces (s)}$. Hence equation of line at first surface is given as:

$$X(1) = X_{\min} \quad (4.1)$$

$$Y(1) = y_0 + t_0 X(1) \quad (4.2)$$

For 2nd surface the equations for X(2), Y(2) and slope t_1 are given as:

$$X(2) = \frac{\left[r_1 + s_1 - t_0 y_0 \mp \sqrt{(r_1 + s_1 - t_0 y_0)^2 - (1 + t_0^2) \{y_0^2 - r_1^2 + (r_1 + s_1)^2\}} \right]}{(1 + t_0^2)} \quad (4.3)$$

$$Y(2) = y_0 + t_0 X(2) \quad (4.4)$$

$$t_1 = \tan \left[\sin^{-1} \left\{ \left(\frac{n_1}{n_2} \right) \sin \left(\tan^{-1} t_0 + \sin^{-1} \left(\frac{Y(2)}{r_1} \right) \right) \right\} - \sin^{-1} \left(\frac{Y(2)}{r_1} \right) \right] \quad (4.5)$$

If we have N surfaces then equations of ray tracing are given as:

$$X(N) = \frac{[r_{(N-1)} + s_{(N-1)} - t_{(N-2)}Y(N-1) + t_{(N-2)}^2X(N-1) \mp \sqrt{A-B}]}{(1 + t_{(N-2)}^2)} \quad (4.6)$$

$$\text{Where } A = [r_{(N-1)} + s_{(N-1)} - t_{(N-2)}Y(N-1) + t_{(N-2)}^2X(N-1)]^2 \quad (4.7)$$

$$B = (1 + t_{(N-2)}^2) \{ [Y(N-1)]^2 - r_{(N-1)}^2 + (r_{(N-1)} + s_{(N-1)})^2 + t_{(N-2)}^2 [X(N-1)]^2 - 2t_{(N-2)}Y(N-1)X(N-1) \} \quad (4.8)$$

$$Y(N) = Y(N-1) + t_{(N-2)}[X(N) - X(N-1)] \quad (4.9)$$

$$t_{(N-1)} = \tan \left[\sin^{-1} \left\{ \left(\frac{n_{(N-1)}}{n_N} \right) \sin \left(\tan^{-1} t_{(N-2)} + \sin^{-1} \left(\frac{Y(N)}{r_{(N-1)}} \right) \right) \right\} - \sin^{-1} \left(\frac{Y(N)}{r_{(N-1)}} \right) \right] \quad (4.10)$$

By following the same approach of forward ray tracing we had derived the formulae for calculation of Xb, Yb and slope tb for backward ray tracing as shown in eq. (4.11), eq. (4.14) and eq. (4.15) respectively.

$$Xb(N) = \frac{[s_{(N-1)} + r_{(N-1)} - Yb(N+1)tb_{(N-1)} + tb_{(N-1)}^2Xb(N+1) \mp \sqrt{Ab-Bb}]}{(1 + tb_{(N-1)}^2)} \quad (4.11)$$

$$\text{Where } Ab = [s_{(N-1)} + r_{(N-1)} - Yb(N+1)tb_{(N-1)} + tb_{(N-1)}^2Xb(N+1)]^2 \quad (4.12)$$

$$Bb = (1 + tb_{(N-1)}^2) \{ [Yb(N+1)]^2 + tb_{(N-1)}^2 [Xb(N+1)]^2 - 2Yb(N+1)tb_{(N-1)}Xb(N+1) + s_{(N-1)}^2 + 2s_{(N-1)}r_{(N-1)} \} \quad (4.13)$$

$$Yb(N) = Yb(N + 1) - tb_{(N-1)}[Xb(N + 1) - Xb(N)] \quad (4.14)$$

$$tb_{(N-2)} = \tan \left[\sin^{-1} \left\{ \left(\frac{n_{(N)}}{n_{(N-1)}} \right) \sin \left(\sin^{-1} \left(\frac{Yb(N)}{r_{(N-1)}} \right) + \tan^{-1} tb_{(N-1)} \right) \right\} - \sin^{-1} \left(\frac{Yb(N)}{r_{(N-1)}} \right) \right] \quad (4.15)$$

If we keep on coming from positive X axis towards negative axis, equations for initial surfaces at the front end are given as:

$$Xb(2) = \frac{[r_1 + s_1 - Yb(3)tb_1 + tb_1^2 Xb(3) \mp \sqrt{Ab - Bb}]}{1 + tb_1^2} \quad (4.16)$$

Where value of Ab when N =2 is given as:

$$Ab = [s_1 + r_1 - Yb(3)tb_1 + tb_1^2 Xb(3)]^2 \quad (4.17)$$

Similarly value of Bb while putting N = 2 is

$$Bb = (1 + tb_1^2)[Yb(3)^2 + tb_1^2 Xb(3)^2 - 2Yb(3)tb_1 Xb(3) + s_1^2 + 2s_1 r_1] \quad (4.18)$$

$$Yb(2) = Yb(3) - tb(1)[Xb(3) - Xb(1)] \quad (4.19)$$

Slope tb_0 for N = 2 is

$$tb_0 = \tan \left[\sin^{-1} \left\{ \left(\frac{n_2}{n_1} \right) \sin \left(\tan^{-1} tb_1 + \sin^{-1} \left(\frac{Yb(2)}{r_1} \right) \right) \right\} - \sin^{-1} \left(\frac{Yb(2)}{r_1} \right) \right] \quad (4.20)$$

After forward and backward ray tracing is done we had obtained equations for Principal planes,

Focal planes and nodal planes which are shown below:

$$(\text{Back Focal Plane})Bf = X(N - 1) - \left[\frac{Y(N-1)}{t_{(N-2)}} \right] \quad (4.21)$$

$$\text{(Back Principal Plane)}B_p = X(N - 1) + \left[\frac{Y(1) - Y(N-1)}{t_{(N-2)}} \right] \quad (4.22)$$

$$\text{(Front Focal Plane)}F_f = X_b(2) - \left[\frac{Y_b(2)}{t_{b_0}} \right] \quad (4.23)$$

$$\text{(Front Principal Plane)}F_p = X_b(2) + \left[\frac{Y_b(N+1) - Y_b(2)}{t_{b_0}} \right] \quad (4.24)$$

$$\text{(Front Nodal Plane)}F_n = F_f + B_f - B_p \quad (4.25)$$

$$\text{(Back Nodal Plane)}B_n = B_f - (F_p - F_f) \quad (4.26)$$

Having all the necessary values of radii of curvature, thicknesses and refractive indices of all refracting surfaces allows us to calculate the equations of lines and subsequently focal planes, principal planes and nodal planes. Nevertheless, also with the help of r , t and n we were able to draw the schematic of an eye as discussed in chapter 2. By fusing both the above steps we were able to build a ray tracing model as shown in figure 4.2. Further with the help of information obtained from this model refractive state and variational analysis of an eye is performed and is discussed in the next chapter.

CHAPTER 5

REFRACTIVE ERROR AND VARIATIONAL ANALYSIS

In the previous chapters we have performed the modeling of an eye where we have extracted all the ocular parameters of an eye such as radius of curvature, thickness of surface and new coordinates of an eye. After calculating all the above mentioned data, schematic of an eye consisting of different layers is plotted for all the specimens of all the strains, as well as average eye of one single strain. Further we have derived the formulae for ray tracing in paraxial model and explained the model when we have perfect eye having zero diopters refractive error.

The next part, which is the most important piece of our work, is to perform ray tracing using all the ocular parameters that has been calculated while modeling of an eye so that we can see the behavior of an eye in realistic world instead of imaginary. Ray tracing would help us to calculate the geometry of an eye, with the help of which we can obtain “Refractive error”. After calculating refractive error we would qualitatively analyze the ocular parameters influencing the refractive error and hence the ocular parameters are categorized as critical or non-critical accordingly.

5.1 Refractive Error

Refractive Error, which is also called as “Ametropia” is usually defined as the deviation of power of an eye from the perfect eye and its value could be zero, positive or negative. Although there are many errors or more precisely disorders that are associated with an eye, but in our scope of work we limit ourselves only to three states of an eye, based on the refractive properties of an eye. Those three conditions are emmetropia, myopia (shortsightedness) and hyperopia (farsightedness).

- **Emmetropia** is a condition when the focus is exactly at the desired place or the rays converge exactly at the photoreceptive part of retina. Thus the $A = 0$ diopters.
- **Myopia** is defined as the disorder associated with an eye where the light rays focuses in front of the retina, hence fall short of the focal point for a perfect eye. Myopia can be treated if we use the lens having negative curvature or more precisely with the concave lens. Figure 5.1 below shows condition of myopia.

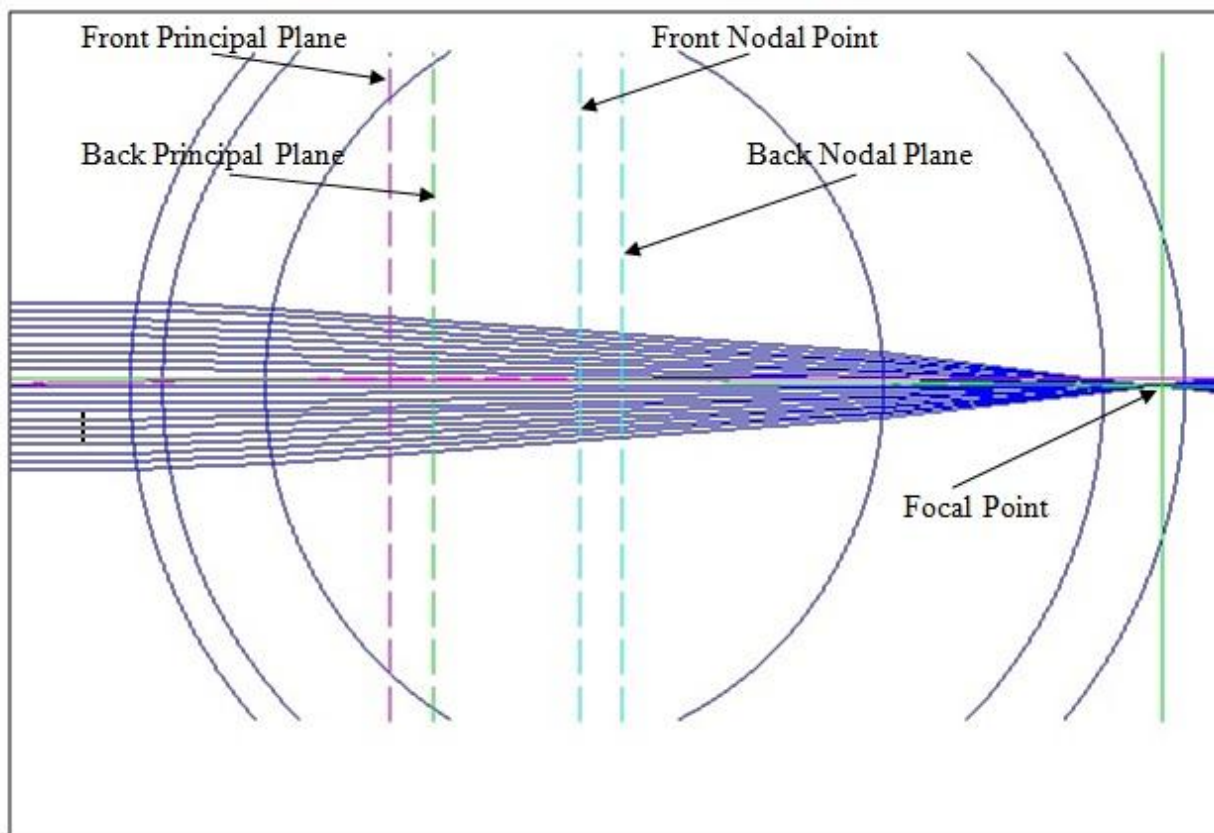


Figure 5.1: Virtual Eye comprising of different layers with condition of myopia.

- **Hyperopia** or farsightedness on the other hand is the disorder of an eye where light rays focuses behind retina. The focal point for this kind of disorder is behind the retina and

could be corrected by using series of convex as well as concave lenses. Figure 5.2 below shows condition of hyperopia.

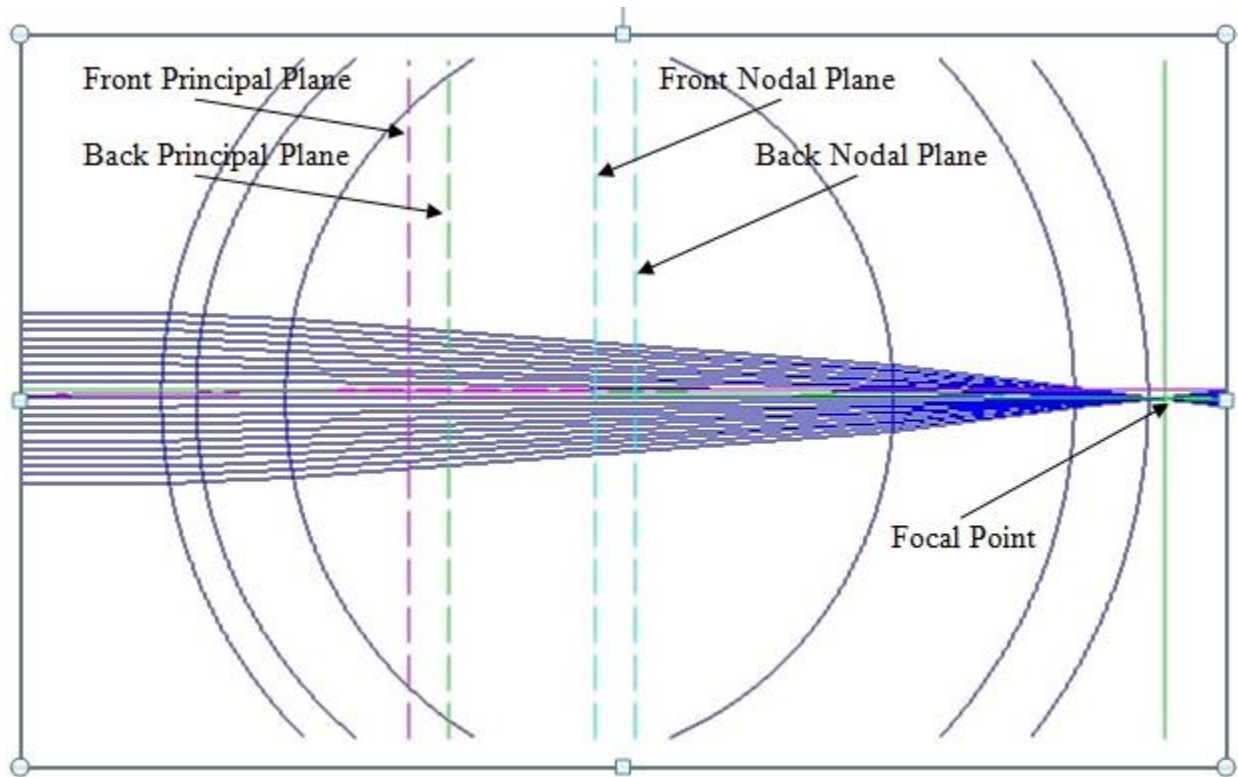


Figure 5.2: Virtual Eye comprising of different layers with condition of hyperopia.

As stated above all the necessary information required for the calculation of the refractive error was extracted from the ray tracing models. By incorporating known values for the optical parameters r , t , s and n in equations (4.1) through (4.20), we were able to calculate X , Y and slope t . Further substituting these values in equations (4.21) through (4.26), we had obtained principal planes and focal planes, which are required for the calculation of the refractive error. Finally, the refractive error of an eye was calculated using Eq. (5.1) below:

$$A = \frac{10^6}{\left[\frac{(Bf - Bp)(-Ff + Fp)}{Bf - S(6)} + Ff - Bp \right]} \quad (5.1)$$

We can see in Eq. (5.1) that all the planes of the geometry that has been calculated are used in calculating the ametropia of an eye and all these planes are calculated from the ocular parameters (r, tt, n) . For this reason we can say that ametropia is a function of 16 ocular parameters that has been already defined in literature and is base line for building our model in order to evaluate ametropia of an eye.

5.2 Variational Analysis

Variational analysis is a method that we have used to qualitatively analyze the effects of minor changes in optical parameters on the refractive error. As the name indicated effects on dependent quantity is observed by varying independent variables. Dependent quantity here implies to refractive error and independent variables are ocular parameters (r, tt, n) . In the variational analysis, only one optical parameter out of the possible 16 parameters is changed and its effect on the refractive error is observed. In schematic of an eye we have 6 refractive layers and other ocular parameters, which are shown in Fig. 4.2. Radius r which is a set of 6 values is expressed as shown below by Eq. (5.2):

$$r = [r_{ac}, r_{pc}, r_{al}, r_{pl}, r_{ar}, r_{pr}] \quad (5.2)$$

In a similar fashion, thicknesses tt and refractive indices n of the refracting surfaces contain 5 elements each and these are represented by Eq. (5.3) and Eq. (5.4) respectively:

$$tt = [tt_c, tt_{aqc}, tt_l, tt_{vc}, tt_r] \quad (5.3)$$

$$n = [n_c, n_{aqc}, n_l, n_{vc}, n_r] \quad (5.4)$$

The concept behind variational analysis is to estimate the effects of r , tt and n on the refractive error when each parameter is incremented by a small variable value. This incremented variable is denoted by “ d ” for r and tt , and “ dn ” for n . While performing variational analysis, we have set the values of d as $1\mu\text{m}$ and dn as 0.001 . For example, if we would like to estimate the effect of the radius of the posterior cornea on refractive state of an eye, the radius of the posterior cornea (r_{pc}) will be incremented by $d = 1\mu\text{m}$ and rest all the parameters will remain unchanged. The set of new elements of r , tt and n are expressed by Eq. (5.5), Eq. (5.6), and Eq. (5.7):

$$r = [r_{ac}, r_{pc} + \mathbf{d}, r_{al}, r_{pl}, r_{ar}, r_{pr}] \quad (5.5)$$

$$tt = [tt_c, tt_{aqc}, tt_l, tt_{vc}, tt_r] \quad (5.6)$$

$$n = [n_c, n_{aqc}, n_l, n_{vc}, n_r] \quad (5.7)$$

Now for an instance if we consider the new calculated value of the refractive error or ametropia, due to change “ d ” in the radius of the posterior cornea r_{pc} is A_2 , then the change in the value of the refractive error due to the change in a single optical parameter r_{pc} is called as the derivative of radius of Posterior cornea and can be represented by Eq. (5.8):

$$dA_{dr_{pc}} = A_2 - A \quad (5.8)$$

This same approach was used to calculate the derivatives for all ocular parameters and estimate the impact of changes in these parameters on the refractive error. Table 5.1 represents all the derivatives and their respective notations.

Refractive Error Components		
Ocular Parameters	Derivatives	Derivative of Ametropia over
1. Anterior Cornea (r_{ac})	$dA_{dr_{ac}} = A1- A$	Radius of Anterior Cornea
2. Posterior Cornea (r_{pc})	$dA_{dr_{pc}} = A2- A$	Radius of Posterior Cornea
3. Anterior Lens (r_{al})	$dA_{dr_{al}} = A3- A$	Radius of Anterior Lens
4. Posterior Lens (r_{pl})	$dA_{dr_{pl}} = A4- A$	Radius of Posterior Lens
5. Anterior Retina (r_{ar})	$dA_{dr_{ar}} = A5- A$	Radius of Anterior Retina
6. Posterior Retina (r_{pr})	$dA_{dr_{pr}} = A6- A$	Radius of Posterior Retina
7. Cornea (tt_c)	$dA_{dtt_c} = A7- A$	Thickness of Corneal
8. Aqueous Chamber (tt_{aqc})	$dA_{dtt_{aqc}} = A8- A$	Thickness of Aqueous chamber
8. Lens (tt_l)	$dA_{dtt_l} = A9- A$	Thickness of Lens
10. Vitreous Chamber (tt_{vc})	$dA_{dtt_{vc}} = A10- A$	Thickness of Vitreous chamber
11. Retina (tt_r)	$dA_{dtt_r} = A11- A$	Thickness of Retina
12. Cornea (n_c)	$dA_{dn_c} = A12- A$	Refractive index of Cornea
13. Aqueous Chamber (n_{aqc})	$dA_{dn_{aqc}} = A13- A$	Refractive index aqueous Chamber
14. Lens (n_l)	$dA_{dn_l} = A14- A$	Refractive Index of Lens
15. Vitreous Chamber (n_{vc})	$dA_{dn_{vc}} = A15- A$	Refractive index Vitreous chamber
16. Retina (n_r)	$dA_{dn_r} = A16- A$	Refractive index of Retina

Table 5.1: Notations for ocular parameters and their respective derivatives.

CHAPTER 6

RESULTS

The previous chapter “Variational Analysis” has completed the targeted work which we have been trying to achieve and set the platform to publish the favorable results. Summarizing our work,

- We have been provided the raw data (X-Y coordinates of different layers of an eye) that acted as a foundation for the “Modeling of an Eye” performed by us. Further with the help of image processing we had visually verified the correctness of 2 dimensional plotting of an eye representing 6 layers of an eye.
- The modeling of an eye performed was not only responsible for generating the schematics but also important ocular parameters (radius of curvature, thicknesses and centers of curvatures etc.) were calculated.
- Ocular parameters in conjunction with the concepts of ray tracing gives us a glimpse of a virtual 2 dimensional model of an eye, where the paraxial rays are passing through different layers of an eye and are converging at definite focal point. This virtual model of an eye helped us to calculate the defects in an eye.
- At last but not the least, infact the most significant part of our work, “Variational Analysis” had been performed, which carved the pathway for performing the qualitatively as well as quantitatively analysis for the optics of an eye.

Since the work was fragmented in sections as summarized above, we would publish our results accordingly. The work performed in sections would be complimented by their respective results in the coming sections.

6.1 Results of Schematic and Geometry of an Eye

This part of the work, with the help of raw points, acted as a foundation for the proceeding chapters. We have generated the schematics of an eye containing 6 layers and all the ocular parameters were calculated. As already mentioned earlier that this task was made possible by use of sophisticated algorithm and program written in MATLAB, the same program was also responsible to store the results in the file in text format automatically. Hence we can say that radii of curvatures, centers of radii of curvatures, new X-Y coordinates, thicknesses of surfaces etc. not only were calculated but also printed in text file without any other effort except the running of program from the MATLAB command window.

6.1.1 Ocular data

Due to big size of the generated text file, we cannot show the entire text file comprising of results of all the strains for each specimen as such in here, but we would show the results in parts. For example figure 6.1 below shows the screenshot for the text file containing the data for the image 1 of specimen M1_L for strain C57BL. In figure 6.1 we can see that date, time, number of input files and particular file to be processed is printed. In result section centers as well as radii of curvatures are printed for all the layers of an eye. New X-Y coordinates are printed as a result of shifting process applied to shift the co-ordinates, such that optical axis of an eye coincides perfectly to the horizontal axis and gives us a good perception of virtual eye. After coordinates comes the R^2 of arc which gives the meaning of how good the fit is. Finally thicknesses or depths of surfaces are printed at the end.

```

Report Started: 18-Apr-2013 10:51:58
Number of input files to process: 4
Input file 1: MRI C57BL P45.xlsx
Number of images in file: 6
Image 1: M1_L_TIF

```

	Cornea_Ant		Cornea_Post		Lens_Ant		Lens_Post		Retina_Ant		Retina_Post	
Center:	(24.6, 1677.3)		(24.6, 1677.3)		(-9.1, 1535.3)		(-2.0, 1127.5)		(6.7, 1674.2)		(-40.5, 1557.2)	
Radius:	1672.4		1576.6		1093.5		1137.7		1294.4		1627.6	
Arc:	X	Y	X	Y	X	Y	X	Y	X	Y	X	Y
	1032.8	343.0	1032.8	465.2	1030.1	1194.8	1003.0	1660.8	1018.5	2481.6	1049.0	2766.4
	938.7	276.8	938.7	392.7	959.8	1028.3	911.2	1806.0	934.7	2576.6	981.1	2824.2
	836.6	215.3	836.6	325.9	873.7	889.9	841.5	1891.0	799.0	2697.9	913.2	2876.1
	734.6	163.1	734.6	269.6	787.5	786.2	743.6	1986.8	679.1	2780.3	815.4	2941.6
	602.5	107.9	602.5	210.4	715.4	716.2	637.8	2068.2	559.3	2844.8	747.5	2981.3
	448.5	59.5	448.5	158.8	599.3	626.7	540.0	2127.8	431.5	2897.0	635.6	3037.7
	286.5	25.5	286.5	122.6	519.2	577.9	428.1	2180.8	267.6	2942.1	515.8	3086.8
	168.5	11.1	168.5	107.3	417.1	528.3	338.2	2213.1	155.7	2960.0	395.9	3125.2
	20.5	4.9	20.5	100.7	263.1	476.2	248.3	2237.3	-0.2	2968.6	262.0	3156.4
	-157.4	14.8	-157.4	111.2	101.1	447.4	144.4	2255.7	-140.2	2960.3	128.1	3176.0
	-313.3	39.4	-313.3	137.3	-68.8	443.5	62.5	2263.4	-280.2	2936.5	2.2	3184.2
	-477.1	81.9	-477.1	182.7	-232.7	464.9	-41.5	2264.5	-390.2	2906.3	-79.8	3184.3
	-619.0	133.7	-619.0	238.1	-374.6	504.7	-145.4	2256.1	-522.2	2855.6	-197.8	3177.1
	-746.8	193.4	-746.8	302.3	-532.3	575.1	-285.4	2229.3	-668.3	2778.7	-315.7	3161.3
	-874.6	267.2	-874.6	382.3	-682.1	673.5	-373.4	2202.8	-770.4	2709.4	-433.7	3136.5
	-980.4	340.6	-980.4	462.6	-787.9	767.8	-483.5	2158.3	-872.5	2624.3	-543.8	3105.0
	-1094.2	434.2	-1094.2	566.4	-917.6	926.8	-607.5	2090.6	-944.6	2552.1	-631.8	3073.6
							-701.7	2024.6	-1016.7	2466.8	-733.8	3029.7
							-795.8	1942.5			-865.9	2959.9
							-889.9	1838.8			-960.0	2900.1
							-946.1	1762.3			-1062.1	2824.2
							-1010.2	1654.6				
R ² of arc:			0.9983		0.9948		0.9885		0.9891		0.9941	
Cornea thickness:	95.8											
Anterior chamber depth:	347.3											
Lens thickness:	1819.7											
Vitreous chamber depth:	693.3											
Retina thickness:	242.9											

Figure 6.1: Summary of the ocular components of specimen M1_L of strain C57BL.

For strain C57BL we have 6 specimen and we shall average the ocular components of all the 6 specimens in order to get the data for one single strain of mouse eye. For convenience we are going to show one more snapshot of the text file representing the ocular parameters. Figure 6.2 show the summary of ocular components for specimen M2_L for same strain i.e. C57BL.

```

Report Started: 18-Apr-2013 10:51:58
Number of input files to process: 4
Input file 1: MRI C57BL P45.xlsx
Number of images in file: 6

Image 2: M2_L_TIF

```

	Cornea_Ant		Cornea_Post		Lens_Ant		Lens_Post		Retina_Ant		Retina_Post	
Center:	(-5.8, 1502.3)		(-5.8, 1502.3)		(-6.0, 1530.8)		(-1.0, 1152.4)		(12.9, 1537.6)		(-13.7, 1624.4)	
Radius:	1504.0		1408.8		1127.2		1115.3		1400.4		1547.8	
Arc:	X	Y	X	Y	X	Y	X	Y	X	Y	X	Y
	1086.0	467.8	1086.0	611.9	1046.4	1127.1	945.8	1741.9	1017.2	2513.5	1064.7	2734.7
	967.6	355.7	967.6	483.8	980.3	985.1	874.9	1842.9	925.1	2600.1	982.5	2809.0
	871.7	280.7	871.7	400.1	914.2	879.9	762.9	1965.1	842.9	2665.5	879.1	2888.7
	764.5	210.5	764.5	322.7	828.3	772.8	650.8	2057.4	718.4	2747.3	765.9	2961.6
	658.6	153.0	658.6	260.0	742.3	687.8	506.4	2145.6	615.1	2801.9	631.4	3031.4
	552.7	105.8	552.7	208.9	646.3	611.5	360.7	2207.4	501.8	2849.9	506.9	3082.0
	425.7	61.5	425.7	161.1	529.2	538.7	236.2	2242.2	356.1	2895.3	351.2	3128.6
	331.0	36.4	331.0	134.3	423.3	488.5	69.3	2265.5	231.5	2920.8	226.7	3153.4
	236.3	17.9	236.3	114.4	307.5	448.0	-77.7	2265.1	85.8	2936.1	59.8	3170.5
	110.5	2.8	110.5	98.3	191.7	421.0	-203.5	2249.2	-218.1	2918.8	-75.9	3170.9
	-15.3	-1.7	-15.3	93.5	23.5	403.9	-361.7	2207.8	-376.3	2882.8	-275.2	3149.9
	-151.0	5.3	-151.0	101.0	-112.2	408.6	-488.7	2155.4	-524.5	2830.8	-412.2	3120.0
	-265.6	20.9	-265.6	117.6	-195.7	419.6	-615.8	2082.9	-630.4	2781.5	-581.7	3064.2
	-370.2	43.1	-370.2	141.4	-341.4	454.6	-744.1	1984.0	-757.5	2707.1	-697.5	3012.9
	-432.5	60.1	-432.5	159.6	-475.9	506.1	-851.3	1874.1	-895.7	2603.2	-835.8	2935.8
	-494.7	80.0	-494.7	181.0	-610.3	579.2	-927.3	1773.5	-1014.1	2489.6	-974.1	2838.2
	-598.1	119.8	-598.1	224.0	-723.6	661.5	-993.4	1661.3			-1102.4	2724.5
	-701.4	168.8	-701.4	277.2	-815.8	746.5	-1059.5	1503.7				
	-814.7	234.3	-814.7	348.9								
	-906.8	298.1	-906.8	419.3								
	-989.0	364.2	-989.0	493.3								
	-1071.2	440.7	-1071.2	580.5								
R^2 of arc:			0.9951		0.9985		0.9957		0.9855		0.9869	
Cornea thickness:	95.2											
Anterior chamber depth:	314.5											
Lens thickness:	1862.3											
Vitreous chamber depth:	678.6											
Retina thickness:	231.0											

Figure 6.2: Summary of the ocular components of specimen M1_L of strain C57BL.

Similarly the data for rest of 6 specimens for mouse strain C57BL can be viewed in the same format. Once we have the ocular data for all the 6 specimens printed, the program would average over all the 6 specimens to give us one set of data representing one single eye for the strain C57BL. Figure 6.3 below shows the ocular data for C57BL.

All Radii:	Cornea_Ant	Cornea_Post	Lens_Ant	Lens_Post	Retina_Ant	Retina_Post
M1_L:	1672.4	1576.6	1093.5	1137.7	1294.4	1627.6
M2_L:	1504.0	1408.8	1127.2	1115.3	1400.4	1547.8
M3_L:	1376.6	1280.6	1210.8	1167.6	1418.9	1633.6
L1_L:	1485.7	1387.5	1160.9	1131.1	1382.7	1488.4
L4_L:	1564.1	1468.3	1264.7	1071.6	1426.2	1517.8
#M1_:	1438.9	1340.3	1167.9	1089.7	1418.0	1486.3
Mean:	1507.0	1410.4	1170.8	1118.8	1390.1	1550.2
Std. Dev.:	102.7	103.2	60.7	34.6	49.4	66.2
Average Eye:						
	Cornea_Ant	Cornea_Post	Lens_Ant	Lens_Post	Retina_Ant	Retina_Post
Center:	(12.3, 1504.4)	(12.3, 1504.4)	(-4.3, 1573.2)	(1.4, 1132.8)	(10.8, 1520.6)	(-14.4, 1600.2)
Radius:	1507.0	1410.4	1170.8	1118.8	1390.1	1550.2
Cornea thickness:	96.6					
Anterior chamber depth:	308.3					
Lens thickness:	1849.2					
Vitreous chamber depth:	659.0					
Retina thickness:	239.7					
Intersection points with optical axis:						
Anterior cornea:	(0.0, -2.5)					
Posterior cornea:	(0.0, 94.1)					
Anterior lens:	(0.0, 402.4)					
Posterior lens:	(0.0, 2251.6)					
Anterior retina:	(0.0, 2910.6)					
Posterior retina:	(0.0, 3150.4)					
Done reading file 1						

Figure 6.3: Summary of the ocular data averaged over all specimens of strain C57BL.

6.1.2 Schematic of an Eye

The ocular data that has been generated acted as an input and schematic of an eye is drawn as shown in figures 6.4 and 6.5. As discussed earlier the ocular data is calculated for individual specimen as well as averaged over all the specimens of single strain, so is the case with the schematic. Schematic of single specimen is drawn using respective ocular data and schematic of average eye of C57BL is drawn as a result of average data for the same.

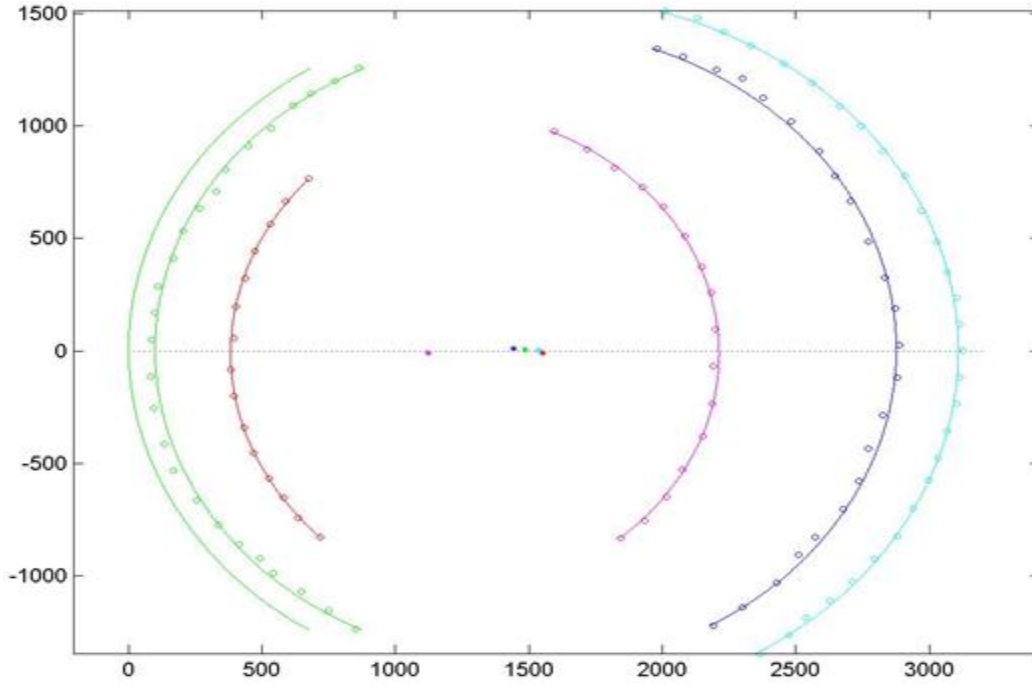


Figure 6.4: Schematic of an eye for specimen M1_L.

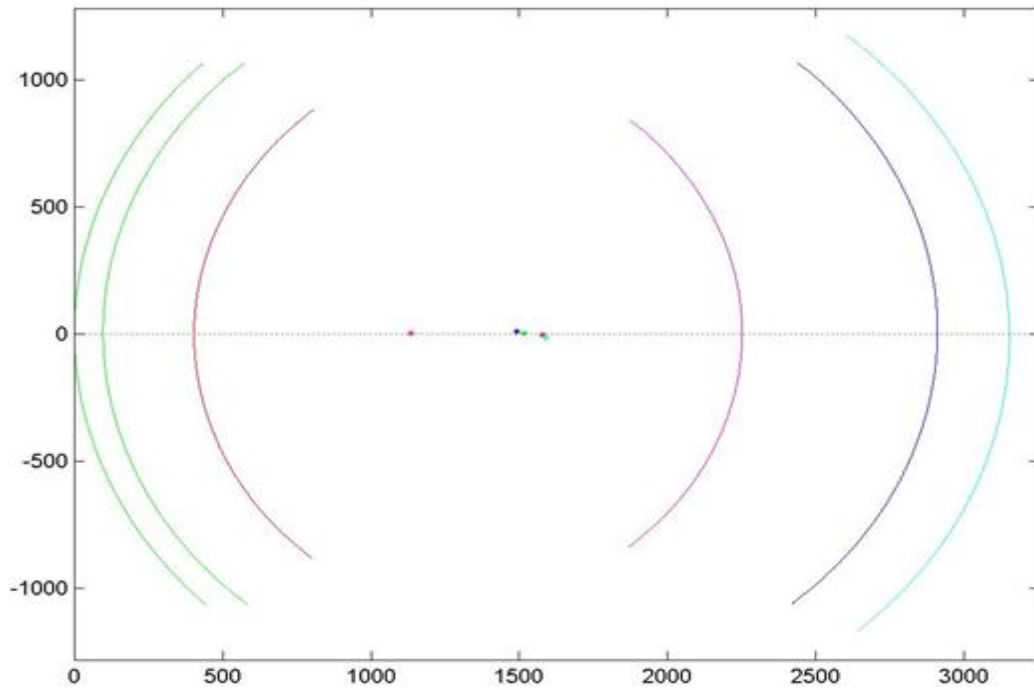


Figure 6.5: Schematic of an eye for C57BL averaged over all the 6 specimens.

6.2 Results of Image Processing

Image processing was performed to visually analyze, how accurate are our generated schematics. In this process drawn schematic of an eye is laid over MRI image of an eye of the respective specimen. Figure 6.6 shows the MRI image of an eye which is provided to us by “School of Medicine”.

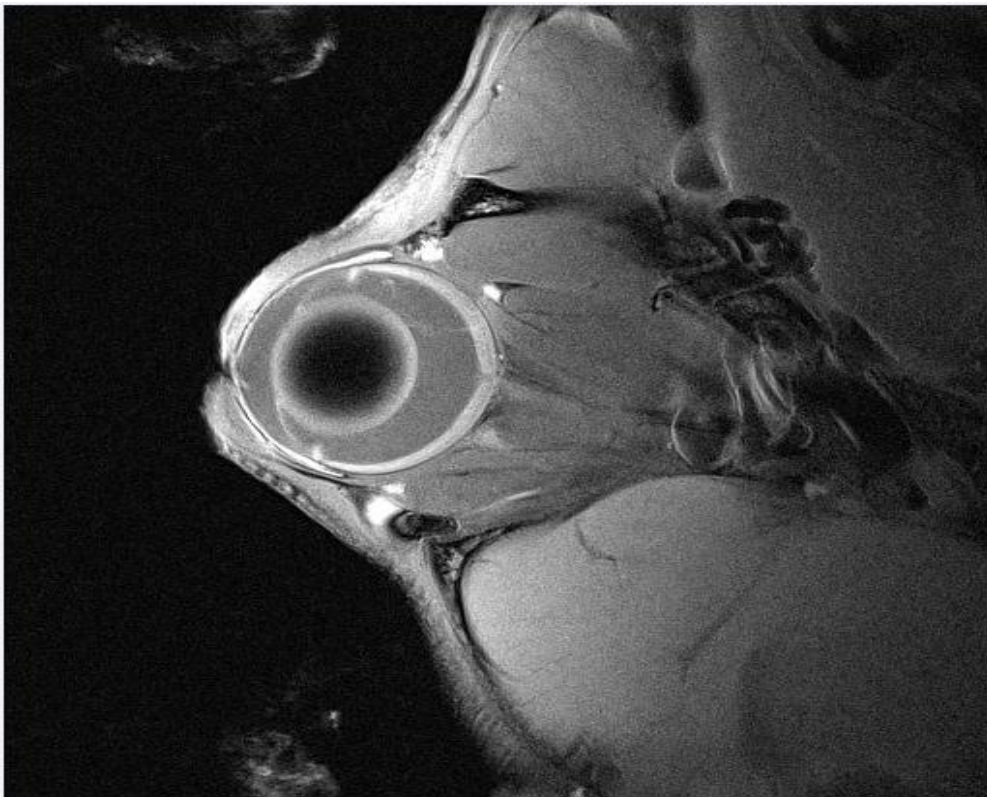


Figure 6.6: MRI image of an eye.

In figure 6.6 along with eye, also surrounding tissues are visible. So the challenge was to draw layers of an eye on top of that image, as we have very poor demarcation of boundaries between the layers. The algorithm generated an image containing different layers of an eye as shown in figure 6.7.

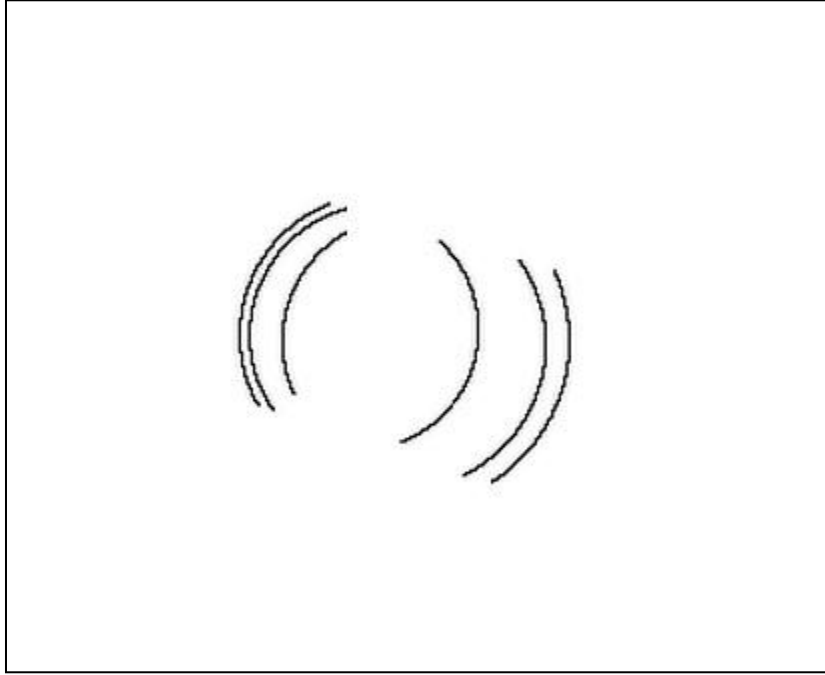


Figure 6.7: 6 different layers of an eye representing schematic of an eye.

Figure 6.8 shows the final outcome of the image processing where layers of an eye (in red) are overlapped over the MRI image of an eye. In order to see the eye only, region of interest was selected and zoomed automatically by program.

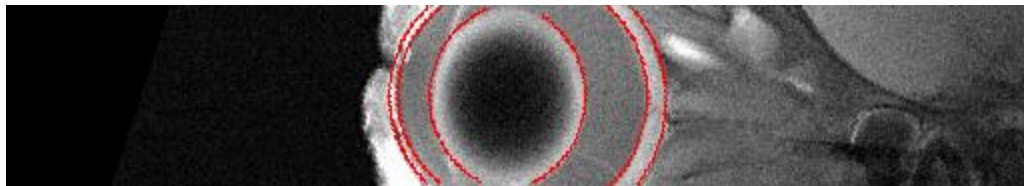


Figure 6.8: Composite image showing the overlapped part in red on top of MRI image.

6.3 Results of Optical Modeling and Ray Tracing

Eventually moving on to next part by confirming our schematics comes the ray tracing. The ray tracing as explained in chapter 4, is performed using the ocular parameters extracted while performing modeling of an eye. This gives us a kind of virtual eye, as if the actual rays are passing through different layers of an eye. By inputting the ocular parameters reported in table 4.1 [3, 4, 5] and 4.2 [6, 7] results are shown below in figure 6.9, 6.10 respectively. The results obtained are eye parameters in paraxial approximation and include front and back focus location, front and back principal plane, front and back nodal point, dioptric strength and ametropia.

```

This file is generated by script EyeDerivatives
Input data from RatEye_650nm.txt
Data for a rat eye from Chaudhyry-1983 at 650nm wavelength

r1 = 3051 - anterior cornea radius, um
r2 = 2959 - posterior cornea radius, um
r3 = 2535 - anterior lens radius, um
r4 = -2441 - posterior lens radius, um
r5 = -3543 - anterior retina radius, um
r6 = -3706 - posterior retina radius, um

t1 = 156 - cornea thickness, um
t2 = 708 - Anterior chamber depth, um
t3 = 3814 - lens thickness, um
t4 = 1409 - Vitreous chamber depth, um
t5 = 217 - retina thickness, um

n1 = 1.0000 - index of medium (air)
n2 = 1.3804 - index of cornea
n3 = 1.3315 - index of Anterior chamber
n4 = 1.6761 - index of lens
n5 = 1.3319 - index of Vitreous chamber
n6 = 1.3319 - index of retina

Eye parameters in paraxial approximation

Xr = 6304.00 - location of back surface of retina, um
Bf = 6488.49 - back focus location, um
Bn = 3042.84 - back nodal point location, um
Fn = 2764.18 - front nodal point location, um
Bp = 1899.10 - back p-plane location, um
Fp = 1620.44 - front p-plane location, um
Ff = -1825.21 - front focus location, um
K = 290.21 - dioptric strength
A = 12.1964 - ametropia

```

Figure 6.9: Summary of eye parameters calculated in paraxial approximation for rat eye [3, 4, 5].

```

This file is generated by script EyeDerivatives
Input data from MouseEye_655nm.txt
Data for a Mouse eye from Remtulla-1984 at 655nm wavelength

r1 = 1517 - anterior cornea radius, um
r2 = 1463 - posterior cornea radius, um
r3 = 1248 - anterior lens radius, um
r4 = -1155 - posterior lens radius, um
r5 = -1643 - anterior retina radius, um
r6 = -1666 - posterior retina radius, um

t1 = 93 - cornea thickness, um
t2 = 452 - Anterior chamber depth, um
t3 = 2032 - lens thickness, um
t4 = 558 - Vitreous chamber depth, um
t5 = 237 - retina thickness, um

n1 = 1.0000 - index of medium (air)
n2 = 1.4015 - index of cornea
n3 = 1.3336 - index of Anterior chamber
n4 = 1.6590 - index of lens
n5 = 1.3329 - index of Vitreous chamber
n6 = 1.3329 - index of retina

Eye parameters in paraxial approximation

Xr = 3372.00 - location of back surface of retina, um
Bf = 3417.53 - back focus location, um
Bn = 1615.00 - back nodal point location, um
Fn = 1551.92 - front nodal point location, um
Bp = 1014.68 - back p-plane location, um
Fp = 951.60 - front p-plane location, um
Ff = -850.93 - front focus location, um
K = 554.72 - dioptric strength
A = 10.7218 - ametropia

```

Figure 6.10: Summary of eye parameters calculated in paraxial approximation for mouse eye [6, 7]

The geometrical parameters that are calculated and shown above for mouse eye and rat eye are calculated by use of paraxial models. On similar lines we have also used the ocular parameters that are calculated by us for different mice strains and geometry of an eye is calculated. Figure 6.11 below shows the geometrical parameters calculated for C57BL mouse strain. While talking of those geometrical parameters, it means for the ametropia (equation 5.1) we need certain planes to be calculated and later incorporated into equation 5.1 to obtain values of ametropia.

```

This file is generated by script EyeDerivatives
Input data from MouseEye_C57BL_510nm.txt
Data for a MouseEye(C57BL) at 510nm wavelength

r1 = 1507 - anterior cornea radius, um
r2 = 1410 - posterior cornea radius, um
r3 = 1171 - anterior lens radius, um
r4 = -1119 - posterior lens radius, um
r5 = -1390 - anterior retina radius, um
r6 = -1550 - posterior retina radius, um

t1 = 97 - cornea thickness, um
t2 = 308 - Anterior chamber depth, um
t3 = 1849 - lens thickness, um
t4 = 659 - Vitreous chamber depth, um
t5 = 240 - retina thickness, um

n1 = 1.0000 - index of medium (air)
n2 = 1.4085 - index of cornea
n3 = 1.3383 - index of Anterior chamber
n4 = 1.6880 - index of lens
n5 = 1.3378 - index of Vitreous chamber
n6 = 1.3500 - index of retina

Eye parameters in paraxial approximation

Xr = 3153.00 - location of back surface of retina, um
Bf = 3081.27 - back focus location, um
Bn = 1466.33 - back nodal point location, um
Fn = 1340.22 - front nodal point location, um
Bp = 900.80 - back p-plane location, um
Fp = 774.69 - front p-plane location, um
Ff = -840.25 - front focus location, um
K = 619.14 - dioptric strength
A = -19.6737 - ametropia

```

Figure 6.11: Summary of eye parameters calculated in paraxial approximation for C57 mouse strain.

6.4 Results of Variational Analysis

The last phase of our work was to conduct qualitatively and quantitatively analysis of refractive state of an eye, which was made possible using concept of “Variational Analysis.” As explained the concept earlier in the chapter 5, the results are quoted in this section. In figures 6.9, 6.10 and 6.11 we have seen that eye parameters are calculated in paraxial approximation and subsequently ametropia is calculated using those eye parameters. The variational analysis is also

performed using ocular parameters, ametropia and the by how much range the ocular parameter should be varied. The results for rat eye [3, 4, 5] and mouse eye [6, 7] are shown in table 6.1 and 6.2 respectively.

Wavelength (nm)		475	500	525	550	575	600	625	650
Refractive error (D) Chaudhuri et al. [5]		+ 6.3	+7.7	+8.7	+9.7	+10.5	+11.2	+11.7	+12.2
Calculated Refractive error (D)		+ 6.3	+7.7	+8.7	+ 9.7	+ 10.5	+11.2	+11.7	+12.2
D E R I V A T I V E S	dA_dr_{ac}	0.0427	0.0428	0.0427	0.0428	0.0428	0.0428	0.0428	0.0428
	dA_dr_{pc}	-0.0057	-0.0057	-0.0056	-0.0057	-0.0057	-0.0057	-0.0057	-0.0057
	dA_dr_{al}	0.0488	0.0485	0.0483	0.0481	0.0480	0.0478	0.0477	0.0476
	dA_dr_{pl}	-0.0083	-0.0082	-0.0081	-0.0081	-0.0080	-0.0080	-0.0079	-0.0079
	dA_dr_{ar}	0.00	0.00	0.00	0.00	0.00	-3.55e ⁻¹⁵	0.00	1.78e ⁻¹⁵
	dA_dr_{pr}	0.00	0.00	0.00	0.00	0.00	0.00	0.00	0.00
	dA_dtt_c	-0.0131	-0.0134	-0.0135	-0.0137	-0.0138	-0.0139	-0.0140	-0.0141
	dA_dtt_{aqc}	-0.0104	-0.0106	-0.0108	-0.0109	-0.0111	-0.0112	-0.0112	-0.0113
	dA_dtt_l	-0.0370	-0.0372	-0.0373	-0.0374	-0.0374	-0.0375	-0.0376	-0.0376
	dA_dtt_{vc}	-0.0697	-0.0695	-0.0694	-0.0693	-0.0692	-0.0692	-0.0691	-0.0691
	dA_dtt_r	-0.0697	-0.0695	-0.0694	-0.0693	-0.0692	-0.0692	-0.0691	-0.0691
	dA_dn_c	0.0016	0.0016	0.0015	0.0015	0.0015	0.0014	0.0014	0.0014
	dA_dn_{aqc}	0.0140	0.0137	0.0136	0.0134	0.0132	0.0131	0.0130	0.0130
	dA_dn_l	-0.3176	-0.3182	-0.3186	-0.3190	-0.3194	-0.3197	-0.3201	-0.3202
dA_dn_{vc}	0.1290	0.1289	0.1288	0.1287	0.1286	0.1286	0.1286	0.1285	
dA_dn_r	0.0119	0.0118	0.0117	0.0116	0.0116	0.0115	0.0115	0.0114	

Table 6.1: Variational Analysis [47] for Rat eye at wavelengths ranging from 475-650nm at a regular interval of 25 nm.

Wavelength (nm)	488	544	596	655	
Refractive error (D) Remtulla & Hallett [6]	-9.4	0.4	6.6	10.8	
Calculated Refractive error (D)	-9.4	0.4	6.6	10.8	
D E R I V A T I V E S	dA_dr_{ac}	0.1748	0.1765	0.1775	0.1783
	dA_dr _{pc}	-0.0315	-0.0308	-0.0309	-0.0312
	dA_dr_{al}	0.1860	0.1798	0.1765	0.1744
	dA_dr _{pl}	-0.0310	-0.0294	-0.0285	-0.0279
	dA_dr _{ar}	3.5e ⁻¹⁵	5.5e ⁻¹⁷	0.00	0.00
	dA_dr _{pr}	0.00	0.00	0.00	0.00
	dA_dtt _c	-0.0473	-0.0511	-0.0535	-0.0552
	dA_dt _{aqc}	-0.0332	-0.0369	-0.0390	-0.0404
	dA_dtt_l	-0.1294	-0.1314	-0.1326	-0.1334
	dA_dtt_{vc}	-0.2455	-0.2428	-0.2412	-0.2401
	dA_dtt_r	-0.2455	-0.2428	-0.2412	-0.2401
	dA_dn _c	0.0041	0.0037	0.0034	0.0032
	dA_dn _{aqc}	0.0156	0.0124	0.0106	0.0093
	dA_dn_l	-0.5971	-0.6004	-0.6027	-0.6042
dA_dn_{vc}	0.1964	0.1946	0.1936	0.1929	
dA_dn _r	0.0496	0.0493	0.0489	0.0486	

Table 6.2: Variational Analysis [47] for Mouse eye at wavelengths 488nm, 544nm, 596nm and 655nm.

Similarly using the ocular data for C57BL mouse strain, referring to figure 6.11 and table 4.3, variational analysis is conducted with the desirable results. Table 6.3 shows the derivatives for

C57BL strain as a result of the variation that is performed in same fashion as is done for table 6.1 and 6.2. We have been given the refractive indices for only two wavelengths (500nm and 510nm) of different media pertaining to different depths of the surfaces.

Wavelength (nm)		500	510
Calculated Refractive error (D)		-21.8	-19.7
D E R I V A T I V E S	dA_dr_{ac}	0.1734	0.1737
	dA_dr_{pc}	-0.0330	-0.0329
	dA_dr_{at}	0.2171	0.2157
	dA_dr_{pt}	-0.0454	-0.0450
	dA_dr_{ar}	6.51e ⁻⁵	7.08e ⁻⁵
	dA_dr_{pr}	0.00	0.00
	dA_dtt_c	-0.0422	-0.0430
	dA_dt_{aqc}	-0.0285	-0.0292
	dA_dtt_l	-0.1322	-0.1326
	dA_dtt_{vc}	-0.2686	-0.2680
	dA_dtt_r	-0.2656	-0.2647
	dA_dn_c	0.0236	0.0235
	dA_dn_{aqc}	0.0083	0.0080
	dA_dn_l	-0.7192	-0.7206
dA_dn_{vc}	0.2680	0.2677	
dA_dn_r	0.0543	0.0545	

Table 6.3: Variational Analysis for C57BL mouse eye strain at wavelengths 500nm and 510nm.

The derivative for each ocular parameter is denoted by a particular notation and is explained in table 5.2. Also certain parameters are contained in red boxes which are crucial and the definition of crucial in concern to the ongoing work is elaborated in the next chapter. All derivatives for the radii of curvature (r), thickness (tt) and refractive indices (n) of various ocular components for the rat and mouse eye at different wavelengths are shown in Tables 6.1, 6.2 and 6.3 respectively. The calculated refractive error values, which are specific to definite wavelength for the rat eye, using ocular parameters from Table 4.1, matches the data reported by Chaudhuri et al. [5] (Table 6.1). Also the refractive error values or ametropia for the mouse eye that has been calculated using data from Table 4.2 is in accordance with the data reported by Remtulla and Hallett [6] (Table 6.2). Similar is the case for C57BL mice strain (data provided by school of medicine), where the refractive error is calculated as shown in table 6.3 using ocular parameters from table 4.3.

Variational analysis [47] revealed that different ocular parameters have different effects on the refractive state of the eye. The refractive indices of the lens and vitreous, as well as vitreous chamber depth and lens thickness have the largest effect on the refractive state of the eye in both rats and mice. The radii of the anterior surfaces of the cornea and lens also have significant impact on the refractive state, while radii of the posterior surfaces of the cornea and lens have much smaller contributions to the refractive state. The radii of the anterior and posterior surfaces of the retina have no effect on the refractive error.

In the rat [5], the relative contribution of ocular components to the refractive state of the eye varied from 0.0697 D per 1 μm for tt_r and tt_{vc} to 0 D per 1 μm for r_{ar} and r_{pr} : $tt_r = tt_{vc} > r_{al} > r_{ac} > tt_l > tt_c > tt_{aqc} > r_{pl} > r_{pc} > r_{pr} = r_{ar}$. The relative contribution of refractive indices in the rat

varied from 0.3176 D per 0.001 units for n_l to 0.0016 D per 0.001 units for n_c : $n_l > n_{vc} > n_{aqc} > n_r > n_c$.

In the mouse [6], the relative contribution of ocular components to the refractive state of the eye varied from 0.2455 D per 1 μm for tt_r and tt_{vc} to 0 D for r_{pr} : $tt_r = tt_{vc} > r_{al} > r_{ac} > tt_l > tt_c > t_{aqc} > r_{pc} > r_{pl} > r_{ar} > r_{pr}$. The relative contribution of refractive indices in the mouse varied from 0.5971 D per 0.001 units for n_l to 0.0041 D per 0.001 units for n_c : $n_l > n_{vc} > n_r > n_{aqc} > n_c$.

The variational analysis is performed for C57BL mouse strain on similar lines as well and the behavior of the refractive state of an eye is observed. This could be accounted for the confirmation for the models built for variational analysis, as is evident by the fact that ametropia calculated by us using variational analysis model is same as reported by [5, 6]. The contribution of ocular components relative to the refractive state of the eye varied from 0.2686 D per 1 μm for tt_{vc} to 0 D for r_{pr} : $tt_{vc} > tt_r > r_{al} > r_{ac} > tt_l > r_{pl} > tt_c > r_{pc} > t_{aqc} > r_{ar} > r_{pr}$. The relative contribution of refractive indices in the mouse varied from 0.7192 D per 0.001 units for n_l to 0.0041 D per 0.0083 units for n_{aqc} : $n_l > n_{vc} > n_r > n_c > n_{aqc}$.

CHAPTER 7

DISCUSSION

In our studies as already discussed, we are concerned about the optics of an eye and the parameters that are responsible for the abnormalities leading to the refractive error. From the class of rodents, mice models are used to study this particular behavior because of genetically engineered models are present in case of mice. Number of mice models [6, 7, 10, 11] are studied and the ocular data has been reported. Also schematics of the mouse eye have been proposed [6]. But still there has been wide variability in the ocular data that has been reported by all the researchers.

Variability has been reported in different strains of mice [12] as well as same strain of mice [11, 12, 13]. Refractive error documented in C57BL/6 mice are close to zero [14-21], where as others say hyperopia or myopia is inherited in same strain of mice [7, 10, 22-24]. Though the variability persists, no one has ever tried to study the factors influencing the variability. We have build our model based on the data provided by “School of Medicine, Wayne state University, Detroit”, for 4 strains of mice C57BL, C57L, CE and CZECH.

7.1 Schematics of an Eye

In this section we have calculated the ocular parameters for all the strains of mice, which are later used for Ray Tracing, calculation of Ametropia and Variational Analysis models. Along with the calculation of parameters also schematics of an eye are generated to give a virtual eye in 2 dimensions. The composite schematics of an eye (raw points represented by small circles and solid line of good curve fitting) generated visually shows that there is minimum error while drawing schematics and the line passes through all the raw points. This is again verified by the

fact that an algorithm which is calculating ocular parameters and generating schematics is also calculating R^2 of arc, which points to goodness of curve. The closer the number to 1, better the fit is. For an instance talking of C57BL mice strain, the data as shown in figure 6.1, those numbers are 0.9883, 0.9948, 0.9885, 0.9891 and 0.9941 for cornea, anterior lens, posterior lens, anterior retina and posterior retina respectively. Thus the fit based on that algorithm is almost perfect.

7.2. Image Processing

This part of our work was performed, in order to further verify that the results (ocular parameters and schematics) obtained from modeling of an eye are correct. We have been given MRI images of different mice strains and were overlapped with the schematics of an eye that are generated while doing modeling of an eye. Figure 3.2 shows MRI image for one of the specimens of C57BL mice strain and figure 3.3 shows the layers of schematic of an eye for same specimen of same strain. A composite image was obtained in which MRI image is used as background and then all the layers represented in red, are drawn on the respective layers of an eye. The visual analysis of composite image 3.5 also shows that the layers are lying exactly over each other with only minor offset at the edges, which could be accounted for the error while obtaining raw points.

7.3. Optical Modeling and Ray Tracing

To meet the eventual and final target of our work, the intermediate step was optical modeling of an eye. In this section the ray tracing is performed using the ocular parameters calculated during modeling of eye. Ocular parameters (listed in table 4.3 for C57BL), that acted

as foundation for the entire work, were inserted in the mathematical model for ray tracing. This ray tracing then calculated the eye parameters, required for obtaining the refractive error or ametropia of an eye. The ametropia calculated, pointed out the defects present in an eye (myopia or hyperopia). This model was verified using the work of [5, 6] for rat and mouse models, where reported ocular parameters (tables 4.1 and 4.2) were inserted in the ray tracing model and the exact refractive error was calculated (figures 6.9 and 6.10)

Quoting an example, ocular components of C57BL (table 4.3) when inserted in ray tracing model, all the eye parameters were obtained (figure 6.11) in paraxial approximation and the refractive state of an eye was inferred. The results have shown that the C57BL mouse eye is hyperopic.

7.4 Variational Analysis

The final goal of our work was variational analysis. It is already emphasized that due to uncertainty that prevails in the available optical models, it is really difficult to quantify the model of the rodent eye. This is accounted for significant swerving in the biometrical parameters even for the same strain of mice [13]. Differences in refractive error are even reported in the most frequently used mouse strain C57BL/6J [13], making it difficult to reconcile existing optical models of the rodent eye with the reported experimental data. Optical modeling of rodents is greatly suffered due to the following reasons:

1. The small size of an eye ball.
2. High power of the rodent eyes.
3. Insufficient resolution of available methodologies for measuring both refractive errors and biometrical parameters in rodents

The challenge that we took in our work is to see that how much changeability in each particular ocular component affects the refractive state as well as calculated refractive error of an eye. Later the Variational Analysis suggests that different parameters have different impact on the refractive state of an eye. The basis of our analysis is as follows.

High-resolution photorefractometry and high-resolution small animal MRI provide the best currently achievable resolution for the rodent eye biometry [18, 20, 22]. The smallest difference in the refractive error (ΔA), which can be identified using high-resolution photorefractometry, is approximately 1.2 D. The smallest difference in the thickness (∂t) of an ocular component, which can be detected by the high-resolution MRI, is approximately 23 μm and the smallest identifiable difference in the radius (∂r) is approximately 26 μm . The variability of the reported refractive indices (∂n) is approximately 0.02. These data can be used to calculate the critical thresholds and identify ocular parameters most affected by the biometrical errors. The critical threshold for the thickness/length of ocular components can be calculated using Eq. (7.1):

$$\text{Threshold (dA_dt)} = \Delta A / \Delta t \quad (7.1)$$

where Δt is the ratio of (∂t) and the incremented thickness (d) of an ocular parameter and is described by Eq. (7.2):

$$\Delta t = \partial t / d \quad (7.2)$$

Substituting values for $\partial t = 23 \mu\text{m}$ and $d = 1 \mu\text{m}$ in Eq. (7.2), gives Δt as shown in Eq. (7.3):

$$\Delta t = 23 / 1 = 23 \quad (7.3)$$

Substituting values for $\Delta A = 1.2$ D, and $\Delta t = 23$ in Eq. (7.1), gives the critical threshold for thickness as shown in Eq. (7.4):

$$\text{Threshold (dA_dt)} = 1.2/23 = 0.0522 \quad (7.4)$$

Thus, the values of dA_dtt above 0.0522 D will identify ocular parameters critically affected by the biometrical errors. Critical thresholds for the radii of curvature and refractive indices can be calculated following similar algorithms and are described by Eq. (7.5) and Eq. (7.6) respectively:

$$\text{Threshold (dA_dr)} = \Delta A/\Delta r = 1.2/26 = 0.0462 \quad (7.5)$$

$$\text{Threshold (dA_dn)} = \Delta A/\Delta n = 1.2/20 = 0.06 \quad (7.6)$$

In our work for variational analysis, optical parameters r, tt are changed by 1 μ m and change in value of refractive indices n is .001. As shown in Tables 6.1, 6.2 and 6.3, experimental errors in ocular biometry and differences in refractive indices for the crystalline lens and vitreous would have the largest impact on the calculated refractive error, whereas errors and differences in refractive indices for the cornea, aqueous and retina would have less significant impact on the refractive error in both mice and rats.

Variation in the thickness/length of the retina and vitreous chamber, as well as in the radius of the anterior surface of the lens, would also significantly affect refractive error in both mice and rats. However, the impact of the differences in the thickness of the lens and radius of the anterior surface of the cornea would be critical only in mice, while the effect on refraction in the rat would be less critical. Changes in other parameters, such as thickness of the cornea, depth

of the anterior chamber, radii of the posterior surfaces of the cornea and lens, as well as radii of the anterior and posterior surfaces of the retina, have very small impact on the refractive error. Variational analysis also revealed that the impact of changes in ocular parameters is substantially higher in the mouse eye compared to the rat eye.

CHAPTER 8

CONCLUSION

There has always been tendency of researchers to look out for the abnormal factors that are making their impact on living or non living models and eventually alteration of their characters leading to change in behavior in the models to make it desirable. In living beings understanding becomes very critical because of the magnitude of masses related directly or indirectly and hence deliberate studies are always required. For the obvious reason therefore researchers always look for models that are genetically identical in terms of organization and various aspects, so that these models acts as a substitute for humans.

Our work has been used to study and understand the optics of the living beings thus rodent models have been studied extensively. Rat and mouse models are increasingly used to study refractive eye development and the development of refractive errors such as myopia. In the small and optically powerful rodent eyes, the precision of biometrical measurements and refraction plays crucial role for optical modeling and obtaining accurate data for the refractive state of the eye.

Our data suggest that not all ocular parameters are critical. Depth of the vitreous chamber, thickness of the lens, radius of the anterior surface of the cornea, radius of the anterior surface of the lens, as well as refractive indices for the lens and vitreous, appear to have the most significant impact on the refractive state of the rodent eye. Developing new methodologies with higher linear resolution for rodent eye biometry and obtaining more accurate data for the refractive indices of the lens and vitreous will help to generate better optical models of the rodent eye.

REFERENCES

1. Stuart Ira Fox, "Human Physiology". Tenth ed. Boston: McGraw Hill; 2008.
2. Xu Cheng, Arthur Bradley, Xin Hong, Larry N. Thibos, "Relationship between Refractive Error and Monochromatic Aberrations of the Eye," *Optometry and Vision Science* VOL. 80, NO. 1, PP. 43–49
3. A. Hughes, "A schematic eye for the rat," *Vision Res* **19**, 569-588 (1979)
4. M. C. Campbell, and A. Hughes, "An analytic, gradient index schematic lens and eye for the rat which predicts aberrations for finite pupils," *Vision Res* **21**, 1129-1148 (1981)
5. A. Chaudhuri, P. E. Hallett, and J. A. Parker, "Aspheric curvatures, refractive indices and chromatic aberration for the rat eye," *Vision Res* **23**, 1351-1363 (1983).
6. S. Remtulla, and P. E. Hallett, "A schematic eye for the mouse, and comparisons with the rat," *Vision Res* **25**, 21-31 (1985)
7. C. Schmucker, and F. Schaeffel, "A paraxial schematic eye model for the growing C57BL/6 mouse," *Vision Res* **44**, 1857-1867 (2004)
8. X. Zhou, P. Bedggood, and A. Metha, "Limitations to adaptive optics image quality in rodent eyes," *Biomed Opt Express* **3**, 1811-1824 (2012)
9. E. G. de la Cera, G. Rodriguez, L. Llorente, F. Schaeffel, and S. Marcos, "Optical aberrations in the mouse eye," *Vision Res* **46**, 2546-2553 (2006).
10. Y. Geng, L. A. Schery, R. Sharma, A. Dubra, K. Ahmad, R. T. Libby, and D. R. Williams, "Optical properties of the mouse eye," *Biomed Opt Express* **2**, 717-738 (2011).
11. G. Zhou, and R. W. Williams, "Mouse models for the analysis of myopia: an analysis of variation in eye size of adult mice," *Optom Vis Sci* **76**, 408-418 (1999).

12. A. V. Tkatchenko, Y. Shen, and T. V. Tkatchenko, "Genetic background modulates refractive eye development and susceptibility to myopia in the mouse," *Invest Ophthalmol Vis Sci* **53**, E-Abstract 3465 (2012).
13. M. T. Pardue, R. A. Stone, and P. M. Iuvone, "Investigating mechanisms of myopia in mice," *Exp Eye Res* (2013)
14. X. Zhou, M. Shen, J. Xie, J. Wang, L. Jiang, M. Pan, J. Qu, and F. Lu, "The development of the refractive status and ocular growth in C57BL/6 mice," *Invest Ophthalmol Vis Sci* **49**, 5208-5214 (2008)
15. X. Zhou, J. An, X. Wu, R. Lu, Q. Huang, R. Xie, L. Jiang, and J. Qu, "Relative axial myopia induced by prolonged light exposure in C57BL/6 mice," *Photochem Photobiol* **86**, 131-137 (2010).
16. X. Zhou, Q. Huang, J. An, R. Lu, X. Qin, L. Jiang, Y. Li, J. Wang, J. Chen, and J. Qu, "Genetic deletion of the adenosine A2A receptor confers postnatal development of relative myopia in mice," *Invest Ophthalmol Vis Sci* **51**, 4362-4370 (2010).
17. Y. Yu, H. Chen, J. Tuo, and Y. Zhu, "Effects of flickering light on refraction and changes in eye axial length of C57BL/6 mice," *Ophthalmic Res* **46**, 80-87 (2011).
18. T. V. Tkatchenko, Y. Shen, and A. V. Tkatchenko, "Analysis of postnatal eye development in the mouse with high-resolution small animal magnetic resonance imaging," *Invest Ophthalmol Vis Sci* **51**, 21-27 (2010).
19. T. V. Tkatchenko, Y. Shen, and A. V. Tkatchenko, "Mouse experimental myopia has features of primate myopia," *Invest Ophthalmol Vis Sci* **51**, 1297-1303 (2010).
20. T. V. Tkatchenko, and A. V. Tkatchenko, "Ketamine-xylazine anesthesia causes hyperopic refractive shift in mice," *J Neurosci Methods* **193**, 67-71 (2010).

21. C. Schmucker, and F. Schaeffel, "Contrast sensitivity of wildtype mice wearing diffusers or spectacle lenses, and the effect of atropine," *Vision Res* **46**, 678-687 (2006)
22. F. Schaeffel, E. Burkhardt, H. C. Howland, and R. W. Williams, "Measurement of refractive state and deprivation myopia in two strains of mice," *Optom Vis Sci* **81**, 99-110 (2004).
23. M. T. Pardue, A. E. Faulkner, A. Fernandes, H. Yin, F. Schaeffel, R. W. Williams, N. Pozdeyev, and P. M. Iuvone, "High susceptibility to experimental myopia in a mouse model with a retinal on pathway defect," *Invest Ophthalmol Vis Sci* **49**, 706-712 (2008).
24. J. Wisard, A. Faulkner, M. A. Chrenek, T. Waxweiler, W. Waxweiler, C. Donmoyer, G. I. Liou, C. M. Craft, G. F. Schmid, J. H. Boatright, M. T. Pardue, and J. M. Nickerson, "Exaggerated eye growth in IRBP-deficient mice in early development," *Invest Ophthalmol Vis Sci* **52**, 5804-5811 (2011).
25. Frank Schaeffel, Adrian Glasser and Howard C. Howland, "Accommodation, refractive error and eye growth in chickens," *Vision Research* Vol. 29, Issue 5 (1988)
26. Frank Schaeffel and Howard C. Howland, "Properties of the feedback loops controlling eye growth and refractive state in the chicken," *Vision Research* Vol. 31, Issue 4 (1991)
27. S. Priolo, J.G. Sivak, E.L. Irving, M.G. Callender, S.E. Moore, "Effect of age and experimentally-induced ametropia on the optics and morphology of the avian crystalline lens," *OSA/VSIA* (1999)
28. A. Hughes and D.I. Vaney, "The refractive state of the rabbit eye: Variation with eccentricity and correction for oblique astigmatism," *Vision Research* Volume 18, Issue 10 (1978)
29. Y. Le Grand and S. El Hage, "Physiological Optics" (Springer, Berlin, 1980)
30. P. Mouroulis, "Visual Instrumentation" (McGraw Hill, New York, 1999)
31. B. H. Walker, "Optical Engineering Fundamentals" (McGraw Hill, New York, 1995)

32. G. Smith and D. A. Atchison, "The Eye and visual Optical Instruments" (Cambridge University Press, Cambridge, 1997)
33. A. Kooijman, "Light distribution of the retina of a wide-angle theoretical eye", *JOSA* **73**, 1544 (1983)
34. R. Navarro, J. Santamaria and J. Bescos, "Accommodation-dependent model of the human eye with aspherics", *JOSA A* **2**, 1273 (1985)
35. I. Escudero-Sanz and R. Navarro, "Off-axis aberrations of a wide-angle schematic eye model", *JOSA A* **16**, 1881 (1999)
36. H. L. Liou and N. A. Brennan, "Anatomically accurate, finite model eye for optical modeling", *JOSA A* **14**, 1684 (1997)
37. E. Nadernejad, S Sharifzadeh and Hamid Hassanpour, "Edge Detection Techniques: Evaluations and Comparisons", *Applied Mathematical Sciences*, Vol. 2, 2008, no. 31, 1507 - 1520
38. S. Dutta and B. B. Chaudhuri, "A Color Edge Detection Algorithm in RGB Color Space", 2009 International Conference on Advances in Recent Technologies in Communication and Computing
39. Mohamed A. El-Sayed, "A New Algorithm Based Entropic Threshold for Edge Detection in Images", *IJCSI International Journal of Computer Science Issues*, Vol. 8, Issue 5, No 1, September 2011 ISSN
40. W. N. Charman, "Optics of Human Eye, Visual Optics and Instrumentation" (CRC Press Boca Raton, 1991)
41. D. Marcuse, "Light Transmission Optics", Van Nostrand Reinhold, New York, 1989

42. R. K. Luneburg, "Mathematical Theory of Optics," University of California Press, Berkeley, 1964
43. M. Kline and I. W. Kay, "Electromagnetic Theory and Geometrical Optics," Interscience Publishers, New York, 1965
44. J. Alda, and J. Arasa, "Paraxial ray tracing," in Encyclopedia of optical engineering (Marcel Dekker, New York, NY, 2004)
45. R. J. Schechter, "Snell's Law: optimum pathway analysis," *Surv Ophthalmol* **21**, 464-466 (1977)
46. J. E. Greivenkamp, "Field guide to geometrical optics", SPIE Press, Bellingham, Wash, (2004)
47. G. Bawa, T. V. Tkatchenko, I. Avrutsky, A. V. Tkatchenko, "Variational analysis of the mouse and rat eye optical parameters", Paper has been sent to *Biomedical Optics Journal* for publication in July 2013. Manuscript ID: 193596.

ABSTRACT**MODELING OF MOUSE EYE AND ERRORS IN OCULAR PARAMETERS
AFFECTING REFRACTIVE STATE**

by

GURINDER BAWA**December 2013****Advisor:** Dr. Ivan Avrutsky**Major:** Electrical Engineering**Degree:** Doctor of Philosophy

Rodents eye are particularly used to study refractive error state of an eye and development of refractive eye. Genetic organization of rodents is similar to that of humans, which makes them interesting candidates to be researched upon. From rodents family mice models are encouraged over rats because of availability of genetically engineered models. Despite of extensive work that has been performed on mice and rat models, still no one is able to quantify an optical model, due to variability in the reported ocular parameters.

In this Dissertation, we have extracted ocular parameters and generated schematics of eye from the raw data from School of Medicine, Detroit. In order to see how the rays would travel through an eye and the defects associated with an eye; ray tracing has been performed using ocular parameters. Finally we have systematically evaluated the contribution of various ocular parameters, such as radii of curvature of ocular surfaces, thicknesses of ocular components, and refractive indices of ocular refractive media, using variational analysis and a computational model of the rodent eye.

Variational analysis revealed that variation in all the ocular parameters does affect the refractive status of the eye, but depending upon the magnitude of the impact those parameters are

listed as critical or non critical. Variation in the depth of the vitreous chamber, thickness of the lens, radius of the anterior surface of the cornea, radius of the anterior surface of the lens, as well as refractive indices for the lens and vitreous, appears to have the largest impact on the refractive error and thus are categorized as critical ocular parameters. The radii of the posterior surfaces of the cornea and lens have much smaller contributions to the refractive state, while the radii of the anterior and posterior surfaces of the retina have no effect on the refractive error. These data provide the framework for further refinement of the optical models of the rat and mouse eye and suggest that extra efforts should be directed towards increasing the linear resolution of the rodent eye biometry and obtaining more accurate data for the refractive indices of the lens and vitreous.

AUTOBIOGRAPHICAL STATEMENT**GURINDER BAWA**

Gurinder Bawa received his Bachelor and Master of Science in Physics (Hons School) from Panjab University, Chandigarh, India, in July 2005. After graduating from physics department, he pursued Masters of Technology in Instrumentation from Panjab University, Chandigarh, India, in July 2007. During his course of study he did number of projects directly or indirectly related to Electronics, Optoelectronics and Image Processing. He worked with the peer group of scientists, who were working in the CERN organization, Geneva, for the “Large Hadron Collider” particle accelerator. He then started his PhD research work in optoelectronics and Image Processing, in Electrical Engineering department at Wayne State University under the guidance of Dr. Ivan Avrutsky. Meanwhile he also graduated with M. S. degree in Electrical and Computer Engineering department with specialization in the field of VLSI. He authored and co-authored 3 journal papers as well as 2 conference papers. He is member of Microelectronics society. He expects to graduate in September 2013.